UNIVERSITÄTSKLINIKUM HAMBURG-EPPENDORF

Klinik und Poliklinik für Neurologie
Prof. Dr. med. Christian Gerloff

Temporal synaptic proteomic changes in the penumbra after ischemic stroke and investigation of Cystatin C as a possible stroke treatment

Dissertation

zur Erlangung des Grades eines Doktors der Medizin
an der Medizinischen Fakultät der Universität Hamburg.

vorgelegt von:

Yuqi Gui
aus Henan, China

Hamburg 2022

(wird von der Medizinischen Fakultät ausgefüllt)

Angenommen von der
Medizinischen Fakultät der Universität Hamburg am:
20.12.2022

Veröffentlicht mit Genehmigung der
Medizinischen Fakultät der Universität Hamburg.

Prüfungsausschuss, der/die Vorsitzende:
Prof. Dr. Eva Tolosa

Prüfungsausschuss, zweite/r Gutachter/in:
PD Dr. Berta Puig

Content

Content **2**

Aims of the study **4**

Introduction **5**

Stroke pathophysiology 5

Excitotoxicity 6

Spreading depolarizations 8

Cerebral edema 8

Oxidative stress 9

Inflammation 10

The concept of penumbra 12

Inflammatory penumbra 14

Treatment for the ischemic penumbra 15

Neuronal communication and stroke 16

The synapse 16

Synaptic damage after stroke 17

Evidence of synaptic recovery after stroke 19

Tools to study the synapsis: the synaptosome 19

Another way of brain communication and therapeutic delivery: Extracellular vesicles (EVs) 20

Materials and Methods **22**

Animals 22

Transient middle cerebral artery occlusion (tMCAO) 22

Isolation of synaptosomes 22

Electron microscopy 23

Electrophoresis and western blot 23

Mass spectrometry 25

In vitro experiments 26

Primary neuronal cell culture 26

Oxygen-glucose deprivation (OGD) 27

Cystatin C treatment 27

Addition of CysC loaded in EVs 28

Cell viability assay 28

Immunocytochemistry 29
Confocal microscopy 30
In vivo experiments 30
Intracerebroventricular injection of EVs loaded with/without CysC 30
TTC staining 31
Immunofluorescence 32
Microscopy 32
Statistical analysis 32
Results 34
Characterization of synaptosomes 34
In vitro experiments results 40
Neurons are still viable 20 min after OGD treatment but synapses are affected 40
Snapses number are decreased 20 min after OGD treatment but rescued by treatment with either recombinant CysC or CysC loaded in EVs 42
In vivo experiments results 45
No differences in stroke volume are observed in mice treated or not with CysC loaded in EVs 24h after injection. 45
No differences in the amount of surviving neurons, and microglia or astrocyte activation in the stroke area after treatments with either non-loaded or CysC-loaded EVs 46
Discussion 48
Stroke and neuroplasticity 48
Proteomic changes after stroke 49
The role of CysC in IS 52
Recombinant CysC could protect neuronal synapses after OGD treatment 53
CysC-loaded EVs may be used as delivery tools as they also protect neuronal synapses after OGD 55
Modulation effect of CysC-loaded EVs in stroked brains 56
Conclusion 57
Summary 58
References 60
Acknowledgment 71
Resume 73
Declaration on oath 74

Aims of the study

Ischemic stroke (IS), which occurs when a cerebral artery is occluded, is the second cause of death worldwide and the major cause of disability (Feigin et al., 2021). The proven treatment of acute IS includes alteplase thrombolysis and endovascular thrombectomy (Phipps and Cronin, 2020, Prabhakaran et al., 2015). However, there is still an urgent need for new therapies as most of the patients are not eligible due to the limited treatment time windows and strict inclusion criteria (only 10-20%) (McMeekin et al., 2017, Boode et al., 2007). A large number of studies were aimed to exploring new therapies for IS, however, bench to the bedside translation has been rather disappointing. Two factors can account for that: on the one hand, the underlying pathological mechanisms are still ill-defined, and on the other hand, it has been shown that some of the most important players have a biphasic nature, detrimental or beneficial depending on the time after stroke (Lo and Ning, 2016). Therefore, the spatiotemporal study of stroke pathology is of utmost importance in the search for new therapeutic tools. The brain functional network is bricked up by neurons and bridged by synapses (Batool et al., 2019). Synapse is the weakest link of the brain network under energy deprivation (Hofmeijer and Van Putten, 2012). IS destroys 14 billion synapses every minute. To compensate for the functional loss, a structural remodelling of the viable tissue surrounding the core of the stroke is settled up (Balbinot and Schuch, 2019), indicating that there are intrinsic surviving pathways that promote neuronal recovery through synaptic dynamics. As synaptic functions are mediated by their protein activities, we are interested in the temporal synaptic protein expression after stroke to gain insight into their intrinsic survival mechanisms. The aims of the present study are: (i) to analyze the dynamics of the synaptic proteomic profile at different time points after stroke in a mouse model. (ii) to identify potential candidates implicated in synaptic survival. (iii) to confirm the candidate(s) potential beneficial role in an *in vitro* and *in vivo* model of stroke.

Introduction

The onset of IS is caused by the formation of a thrombus or an embolism in the brain vessels, which suddenly blocks the blood flow leading to energy deprivation in the corresponding brain area, eventually causing brain cell death and neurologic function defects. During the vascular obstruction, the damage to the brain in the central area of the infarction is irreversible, while the brain area surrounding the infarct core (the penumbra) is functionally depressed due to reduced blood flow, but the damage is still reversible within a limited time window (D'Ambrosio et al., 2001). Among patients with acute stroke, for those who still show perfusion-diffusion mismatch on neuroimaging (meaning tissue that is still viable, thus looks normal on diffusion-weighted imaging, but shows blood hypoperfusion on perfusion-weighted imaging), the most urgent goal of treatment is to rescue the penumbra as much as possible, which can directly decrease long term disability (Lin and Liebeskind, 2016). There are some inherent neuronal repairing mechanisms after stroke, however, how they exactly work is still elusive. It is of utmost clinical significance to find novel therapeutic methods through further investigation of the pathophysiologic changes in the penumbra area, in order to make up for the insufficiencies of current treatments.

Stroke pathophysiology

Stroke pathophysiology is very complex and involves several players. Briefly, the lack of glucose and oxygen leads to a decrease in cellular ATP and an increase in the intracellular calcium concentration increase, leading to a release of glutamate, which will cause excitotoxicity and spreading depression all over the affected area. The blood brain barrier (BBB) is disrupted because of the activity of metalloproteinases activated by free radicals, the ionic imbalance, and the modification of the tight-junction proteins, leading to brain edema thus negatively influencing perfusion. As a consequence of the upregulation of nitric oxide synthases activity in brain cells and the disruption of the mitochondrial electron transport chain after brain ischemia, there is oxidative stress inducing the production of free radicals including reactive oxygen species (ROS) and

reactive nitrogen species (RNS), which break cell membranes, mitochondria, and DNA (Love, 1999). Furthermore, molecules released from damaged cells, such as ATP, behave as danger associated molecular patterns (DAMPs) recruiting the inflammatory cells to the affected brain area, leading the ischemic cascade into the neuroinflammatory phase. Finally, in the chronic phase of stroke, it starts the tissue repair and regeneration and determines the outcome of stroke (Ceulemans et al., 2010). Thus, multiple players are involved in the stroke pathophysiology, such as excitotoxicity, inflammation, mitochondrial stress, free radicals release, protein misfolding, etc. However, some molecules are involved in both stroke pathology and recovery. To design a neuroprotective therapy we may promote internal recovery mechanisms, and interrupt the self-damaging cascade (George and Steinberg, 2015). To accomplish that goal, it is imperative to get a deeper understanding of the stroke pathophysiology. In the following paragraphs, I will describe in more detail what is known about the pathological mechanisms of stroke.

Excitotoxicity

NMDA receptor (NMDAR) is, together with the AMPA (α-Amino-3-hydroxy-5-methyl-4-isoxazole propionic acid) and the kainate receptors, the ionotropic glutamate receptors of the central nervous system (CNS). They mediate excitatory postsynaptic transmission. NMDAR activation requires two coagonists (glutamate and glycine) (Benveniste and Mayer, 1991), they are composed of subunits, GluN1/2/3, and each has different isoforms (e.g., GluN1-1b; GluN2A-D; GluN3A-B), modulating the structure and function of NMDAR. Functional NMDA receptors are the combination of two obligatory glycine-binding GluN1 subunits and two glutamate-binding GluN2 and/or glycine-binding GluN3 subunits. GluN1 and GluN2 subunits mainly affect the intramolecular domain structure, the potency of glutamate, and the duration of excitatory postsynaptic current (EPSC). The physiological significance of GluN3 remains elusive (Vyklicky et al., 2014).

NMDARs can be localized either at the synapsis or extra-synaptic. Synaptic NMDARs

activate cellular defense against oxidants and suppress pro-apoptotic pathways, while the extra-synaptic NMDARs promote pro-apoptotic pathways (Léveillé et al., 2010). These two types of localization also exert opposing functions in stroke. The synaptic NMDAR activity promotes neuronal survival in stroke through promoting cAMP-response element binding protein (CREB) dependent gene expression, which in turn suppresses the expression of pro-apoptotic genes. Whereas extra-synaptic NMDAR activation inhibits CREB activation (Kaufman et al., 2012). Moreover, the subunits composition of NMDARs also determines their role in stroke. The activation of GluN2A-containing NMDAR activation tends to promote ischemic tolerance by inducing CREB activation and thereby alleviating ischemic injury, whereas GluN2B-containing NMDAR activation activates the necrotic cell death program and thus aggravating stroke damage (Y. Liu et al., 2007, Chen et al., 2008, Terasaki et al., 2010, X. Zhang et al., 2015). During the acute phase of ischemia, a sudden rise of the extracellular glutamate concentration and stimulation of the GluN2B-containing NMDARs in the extra-synaptic sites triggers excitotoxic neuronal death (Lai et al., 2014). The specific coupling of GluN2B with postsynaptic density-95 (PSD95) mediates the neurotoxicity of NMDAR through Ca^{2+} influx-induced nitric oxide (NO) production (Sattler et al., 1999). These opposite roles could be explained because GluN2B-containing NMDARs preferentially localize at the extra-synaptic sites, which is in agreement with the finding that in the adult brain, GluN2B-containing NMDARs are enriched in the extra-synaptic sites, whereas GluN2A-containing NMDARs are mainly expressed at the synapse (Wu and Tymianski, 2018). The complexity and dual effects of NMDARs activation might be the explanation for the invalidation of a long list of drugs targeting glutamate receptors when assessed in clinical trials (Chamorro et al., 2016). However, the PSD95 inhibitor, NA-1 (tat-NR2B9c), which selectively perturbs the downstream mechanism of NMDAR neurotoxicity without affecting normal glutamate receptor function, seems to be promising in protecting against stroke injury (Ballarin and Tymianski, 2018, Xu et al., 2016).

Spreading depolarizations

Microinjection of $3.4*10^{-8}$ mol KCL solution to around 1 mm^3 in the rodent cerebral cortex is enough to trigger neuronal depolarization that leads to K^+ and glutamate neuronal efflux, while Na^+ and Ca^{2+} influx to the cell (Matsuura and Bureš, 1971). The transmembrane ion shifts initiate the same depolarization cycle in adjacent cells and thus spreading the depolarization propagation from the center of the stimulus to the peripheral tissue. This process is termed spreading depolarization (SD) and propagates at a rate of 2-9 mm per minute (Woitzik et al., 2013). Due to the fact that self-correction mechanisms for this ion homeostasis disturbance are energy-consuming, as it needs the activity of the Na^+-K^+-ATPase activity and reuptake of excitatory neurotransmitters by astrocytes, in the penumbra, this depolarization will become sustained and the energy supply-demand mismatch will be aggravated (Ayata and Lauritzen, 2015). Thus, elevated intracellular Ca^{2+} concentration and excessive glutamate receptor activation leading to SD cause cell death. In turn, spreading depression of neuronal electrochemical activity will happen as a secondary epiphenomenon to SD, leading to corresponding neurological deficits (Dreier, 2011). In ischemic cerebral tissue, SD could lead to a dramatic elevation of extracellular K^+ concentration, which is vasoconstrictive (Golding et al., 2001). As a result, it forms a vicious cycle where stroke causes spreading depolarization, while in the penumbra area, spreading depolarization tends to be sustained because of energy-deprivation, and leads to spreading ischemia due to its vasoconstrictor effects, finally causing cell death.

Cerebral edema

As cell depolarization happens, the ion transporters on endothelial cells fail to maintain ion and water homeostasis, and the influx of Na^+ and Ca^{2+} will absorb water into intracellular space, leading to cytotoxic edema. Shortly after that, the activation of matrix metalloproteinases (MMPs) and reactive oxygen species (ROS) production initiate the degradation of endothelial glycocalyx and the reduction and redistribution of endothelial junctional proteins such as occludins and claudins, disrupting the BBB (Nian et al., 2020). Increased BBB permeability leak fluid from blood vessels into the

brain extracellular compartment, causing vasogenic cerebral edema. Increased intracranial tissue volume dramatically increases intracranial pressure resulting in further cellular damage caused by brain tissue compression, and brain stem dysfunction caused by transtentorial and uncal herniation, which might need surgical cranial decompression to relieve the effects of increased intracranial pressure (W. D. Heiss, 2016). Due to the brain damage produced in severe ischemic edema, therapies that target relieving brain edema have been explored. Aquaporin-4 (AQP4) distributes all over the astrocytic foot processes that are part of the BBB and the ependymal cell membranes in the brain, it allows bidirectional water transportation through cellular membranes. It plays an important role in brain edema, which is consisted of two parts, initial cytotoxic edema (cellular edema) and vasogenic edema (the volume increase of extracellular fluid, caused by BBB damage). Phenotypic analysis of AQP4-deficient mice demonstrated that AQP4 aggravated cytotoxic edema but helped to relieve vasogenic edema in IS. Interfering with the expression of AQP4 on astrocytic foot processes seems to be a rather promising therapy since it avoids changing AQP4 expression in other tissues (Manley et al., 2009). Drugs like Goreison and Avorvastatin have been tested to suppress AQP4 expression and therefore to decrease the brain edema in the early phase of IS, with positive results in a mouse model (Nakano et al., 2018, Cheng et al., 2018). Besides, therapeutics aiming at restoring BBB structure and function are also explored but they still need further investigation (Nian et al., 2020).

Oxidative stress

Shortly after ischemia happens, the mitochondrial respiratory chain is inhibited due to the lack of oxygen and glucose, leading to ATP depletion and membrane depolarization. To obtain energy, glycolysis is put in place, leading to the production of lactic acid and acidification of the cytoplasm. As a consequence, some physiological metabolism reactions are inhibited and ROS generation is increased . Reperfusion will worsen the damage as it will induce large amount of ROS generation due to oxygenation increment (Orellana-Urzúa et al., 2020). Oxidative stress is also partially the consequence of excitotoxicity, as glutamate-induced Ca^{2+} influx can activate cyclooxygenase,

phospholipase, and nitrite oxygenase, fostering free radicals production (Chamorro et al., 2016). The radicals generated (e.g., hydrogen peroxide, hydroxyl radical, nitric oxide, and peroxynitrite) can cause direct damage to all components of cells, including DNA, proteins, and lipids, leading to massive cellular autophagy, apoptosis, and necrosis (P. Li et al., 2018). It can also promote the release of many proinflammatory cytokines and chemokines and the expression of adhesion molecules on the endothelial cell surface, which eventually leads to leukocytes' migration to the brain parenchyma (Orellana-Urzúa et al., 2020). Antioxidant agents, such as NADPH oxidase inhibitors, xanthine oxidase inhibitors, and polyphenol have been proven to reduce ischemic damage in rodent stroke models. Vitamin C and E, two potent antioxidants in humans, have been proved to be protective in clinical treatment for IS by scavenging ROS, with vitamin E being more effective as it is lipid soluble and thus has better absorbance by the brain (Rodrigo et al., 2013).

Inflammation

In general, following acute IS, resident microglia and astrocytes are activated by DAMPs and cytokines released from damaged cells, and subsequently produce pro-inflammatory mediators, which attract inflammatory neutrophils, lymphocytes, and monocytes into the ischemic tissue (Ceulemans et al., 2010). Interestingly, this secondary neuroinflammation promotes further ischemic injury but also plays a beneficial role (Jayaraj et al., 2019). Shortly after stroke onset, activated macrophagic microglia migrate towards the ischemic lesion to clear necrotic debris and harmful components. However, excessive microglia activation also leads to severe secondary inflammatory injury causing BBB disruption, oxidative stress, and neurogenesis (neuronal formation) inhibition (T. Li et al., 2021). A current widely accepted view is that, in response to ischemic insult, microglia are rapidly activated to differentiate into either the M1 or the M2 phenotype, which are involved in tissue damage and repair, respectively (Jiang et al., 2020; Xiong et al., 2016; Qin et al., 2019). Astrocytes, on the other hand, provide structural and functional support for neurons under physical conditions, but also play a dual role after ischemic insults. In response to all forms of

CNS injury and diseases, astrocytes become reactive astrocytes, exhibiting morphological and functional changes. Upregulation of two intermediate filament (IF) proteins, the glial fibrillary acidic protein (GFAP) and vimentin, is the hallmark of reactive astrocytes (L. Li et al., 2008). In the analogy to microglia, there are at least two types of activated astrocytes, termed A1 and A2. The A1 subtype is considered to be induced by activated microglia and can upregulate members of the complement systems and proinflammatory genes, previously shown to damage synapses, while the mechanism that induces A2 might be related to p38 mitogen-activated protein kinase (MAPK) activation in astrocytes triggered by proinflammatory cytokines, but contrary to A1, they upregulate many neurotrophic factors and thus be beneficial (Liddelow and Barres, 2017).

In response to the proinflammatory factors released from the ischemic lesion, neutrophils are attracted to infiltrate into the brain parenchyma (especially at the margin of the stroke area) minutes to hours after stroke under BBB hyperpermeability condition (Perez-de-Puig et al., 2015, Jin et al., 2010). Neutrophils play an important role as they release neutrophil extracellular traps (NETs), a usual mechanism to trap pathogens. An extracellular stimulus such as bacterial infection or cytokines released from injured cells can activate neutrophils, causing a rise of intracellular calcium that contributes to exocytosis of intracellular granules, in a process called neutrophil degranulation. These granules are released in a hierarchical manner and enriched with myeloperoxidases (MPO), matrix MMPs, gelatinase, neutrophil elastase (NE), and many other proteases, whose initial function is to eliminate pathogens but in the meantime they contribute to extracellular matrix breakdown and vascular damage, and hypoxia will augment neutrophil degranulation and drive more tissue damage (Lodge et al., 2020). In stroke, NETs are web-like structures, induced by the ROS released from mitochondria or produced by NADPH oxidase. They are composed of cytosolic and granule proteins (histones, neutrophil elastases, and MPO) that are assembled on a scaffold of decondensed chromatin (Papayannopoulos, 2017). NETs can inhibit revascularization

and functional recovery after stroke, as it has been shown that inhibiting one of their upstream promoters can improve vascular repairment (Kang et al., 2020). HMGB1, a DAMP molecule released by dying neurons, can induce neutrophils to release NETs. Both HMGB1 and NETs levels are found elevated in the peripheric circulation and CNS after stroke, thus forming a vicious circle where HMGB1 aggravates NET-mediated neuronal death causing more HMGB1 production (S. W. Kim et al., 2019). However, neutrophil infiltration after stroke can also decrease vascular permeability and is involved in angiogenesis through the generation of MMPs (Easton, 2013).

Circulating T cells start to infiltrate into the infarct area relatively later, from around 3-4 days after stroke until 7 days. Different subtypes of T cells have discrete roles in stroke pathogenesis. For instance, CD8+ T cells and CD4+ TH1 cells contribute to the inflammatory response and neurological deficits. However, CD4+ TH2 cells have a protective function by secreting anti-inflammatory cytokines. Regulatory T cells (T_{reg} cells) play an immunological regulatory role by antagonizing the production of TNF-α and IFN-γ. As for γδT cells, though there is a minor part of T cells, (Shichita et al., 2009) increase activity and numbers in the peripheral and the boundary infarct area after ischemia/reperfusion (I/R) damage 4 days after stroke. γδT cells are a source of the interleukin-17 (IL-17) which promotes an inflammatory response after stroke. Therefore, their inhibition might be a therapeutic target for delayed neuronal cell death in stroke (Jin et al., 2010).

The concept of penumbra

After a brain artery is occluded, the affected brain area is artificially divided into two subareas referring to the influx of cerebral blood flow (CBF). The infarct core, where the brain parenchyma lack blood flow, is the most severely affected area in which rapid neuronal death is ongoing. The penumbra surrounds this area and is hypoperfused. Here, neurons are functionally silent but structurally intact and viable, so if the ischemia is corrected in time, the penumbra could still be rescued. Otherwise, the penumbra will transit to the infarct core (usually in less than 24 h) (Saver, 2006). The penumbra was

first defined in 1977, by Astrup *et al.* while performing electrophysiological recordings in baboons. They could show that, when the CBF dropped to around 0.20 ml/g/min, the neuronal electrical activities in the penumbra were compromised, and disappeared at around 0.15 ml/g/min, although at that point the extracellular potassium concentration was only slightly elevated, indicating cellular viability was not compromised. When the CBF continued to decrease to a range between 0.06-0.10 ml/g/min, the extracellular potassium increased sharply, implicating neuronal membrane failure. Massive neuronal death happened when CBF dropped below 0.06 ml/g/min (Astrup et al., 1977) (Figure 1).

It is noteworthy to highlight that this binary definition simplifies the real pathophysiological situation. On the one hand, different neurons vary in their vulnerability to ischemia, thus the boundary between the penumbra and infarct core becomes naturally blurred (Back, 1998). On the other hand, the CBF thresholds are different among the species. Based on experimental studies in animals, 0.17 and 0.10 ml/g/min are two threshold values routinely used to discriminate between the normal brain tissue (> 0.17 ml/g/min), the penumbra (0.10-0.17 ml/g/min), and the infarct core (< 0.10 ml/g/min) (Latchaw et al., 2003). Yet in humans, according to a systematic review, the CBF threshold values defining penumbra and infarct core have high variability, ranging from 0.14-0.35 ml/g/min as the upper CBF threshold for penumbra, and approx. 0.05-0.08 ml/g/min for the infarct core (Bandera et al., 2006). Moreover, the persistence of ischemic penumbra is dependent not only on the CBF but also on the ischemic time duration. The longer the brain tissue is nutrition-deprived, the higher must be the CBF threshold to maintain the capacity for the tissue to be rescuable. For instance, in cats, the penumbra can persist for 25, 40, and 80 min with a CBF at approximately 0, 0.10, and 0.15 ml/g/min, respectively (Heiss and Rosner, 1983).

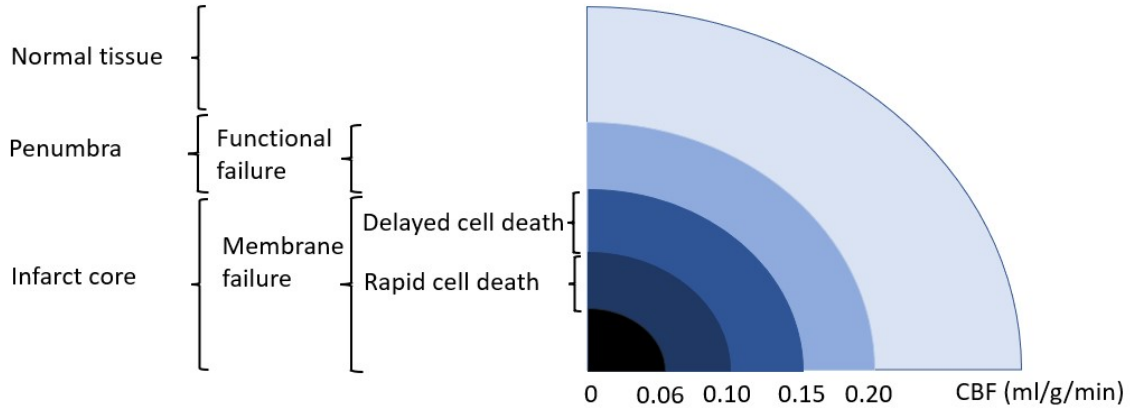

Fig. 1. Cerebral blood flow related to viability of neurons in baboons as described by Astrup et al., 1977. When CBF is above 0.15 ml/g/min, the viability of neurons are still sustained, otherwise, the membrane failure happens and cell death program is activated.

Since the neuronal damage in the penumbra is still reversible, it has been the main battleground for diagnostic, prognosis, and therapeutic intervention for the past several decades. There are multiple kinds of neuroimaging modalities for penumbra mapping, including magnetic resonance imaging (MRI), computed tomography (CT), and positron-emission tomography (PET) technologies. Perfusion-weighted MRI (PWI) provides the hemodynamic imaging of perfusion compromised areas, within which the brain tissue damage could be defined as still reversible or not. Diffusion-weighted MRI (DWI) or PET provides information on the bioenergetic compromised area. The mismatch between the hemodynamically compromised area and the energy metabolism disrupted area should equal the penumbra area. Perfusion CT can also estimate the penumbra area, the cerebral blood volume (CBV), CBF, mean transit time (MTT), and time-to-maximum (Tmax) images derived from perfusion CT are very useful to accurately calculate the penumbra volume (S. H. Yang and Liu, 2021, Fisher and Bastan, 2012).

Inflammatory penumbra

Lately, with the increased knowledge about the pathophysiological process and therapeutic options, the concept of “inflammatory penumbra” has emerged. Preclinical studies demonstrated the presence of a secondary lesion growth between 24h and 7 days after stroke onset which was mediated by the deleterious effects of cytotoxic T-cells

entering the penumbra in a CD49d/vascular-cell adhesion molecule-1 (VCAM-1)-dependent manner (Liesz et al., 2011, Gauberti et al., 2013). This was defined as the inflammatory penumbra, an area at risk surrounding the infarct core, populated by infiltrating T cells, that can be rescued by immunomodulatory treatments (in contrast to the reperfusion treatment necessary for the rescue of the ischemic penumbra at the acute phase of stroke), occurring at the subacute phase of stroke (Llovera et al., 2015). Although the attempt to treat IS in the acute phase with anti-inflammatory drugs has failed (del Zoppo, 2010), immunomodulatory treatments restraining the entry of blood lymphocytes into the brain gained significant effect between 24h to 7 days poststroke both in animal and clinical experiments (Llovera et al., 2015). Due to the huge breakthrough in neuroimaging techniques in recent years, it is now possible to visualize the inflammatory penumbra by targeting VCAM-1 in high-resolution molecular MRI (Gauberti et al., 2013). Despite the promising prospect of anti-inflammatory treatment against inflammatory penumbra, it has to be taken into account the increased risk of poststroke infection, together with the inhibition of the protective effects of the inflammatory reactions as described above (Gauberti et al., 2016).

Treatment for the ischemic penumbra

As mentioned above, the recombinant tissue plasminogen activator (rtPA) thrombolysis treatment has been the only effective drug therapy minimizing the penumbra evolvement into infarct core, despite its low eligibility, limited therapeutic window (4.5 h after stroke), and high risk of causing hemorrhagic transformation. However, modern neuroimaging modalities are capable of discriminating salvageable penumbra from infarct core, and the treatment time window could be extended to 12 h after stroke (Paciaroni et al., 2009, Rabinstein, 2020). Mechanical thrombectomy is another therapy that can initiate reperfusion and rescue the penumbra within 6 h after stroke. Encouragingly, two clinical endovascular treatment trials including patients up to 24 h after stroke onset presenting a “tissue window” (existence of penumbra on neuroimaging) showed significant improvement in the mechanical thrombectomy group compared to patients who only received standard treatments (Silva and Nogueira, 2020).

Many efforts have been made in the investigation of stroke pathophysiology. The current review is that, apart from focusing on the restoration of CBF, the concept of neuroprotection has evolved, presenting the protection of the neurovascular units, composed of vascular cells, glial cells, and neurons, and the improvement of their interactions could possibly surpass the limitation of the current therapeutic window. Neuroprotection therapy alone has not been proven to be effective in rescuing penumbra (R. Liu et al., 2012).

Neuronal communication and stroke

The synapse

Synapses are the communication channels between neuronal cells. A synapse consists of the presynaptic part, the synaptic cleft, and the postsynaptic membrane (Figure 2). The presynaptic part is located on the neuronal axonal end foot and is filled with synaptic vesicles containing neurotransmitters. When a neuronal electrical signal reaches the presynaptic membrane, the voltage-gated calcium channels open to allow Ca^{2+} influx. Increased intracellular calcium concentration induces the phosphorylation of synapsins, synaptic vesicular proteins, which undock the synaptic vesicles from their reserve pool, which then go to the presynaptic active zone where they fuse with the plasma membrane, releasing the neurotransmitters into the synaptic cleft (Hofmeijer and Van Putten, 2012). The neurotransmitters bind then to their receptors on the postsynaptic membrane located on the dendritic spine or neuronal body of the recipient neuron inducing there an electrical response. In glutamatergic synapses, the postsynaptic density (PSD) opposing to the presynaptic active zone, anchored to the postsynaptic membrane, is an electron-dense area composed of hundred scaffold proteins, neurotransmitter receptors, ion channels, adaptor proteins, and signaling molecules which seems to be of utmost importance in synaptic plasticity and synaptic regulation (Boeckers, 2006).

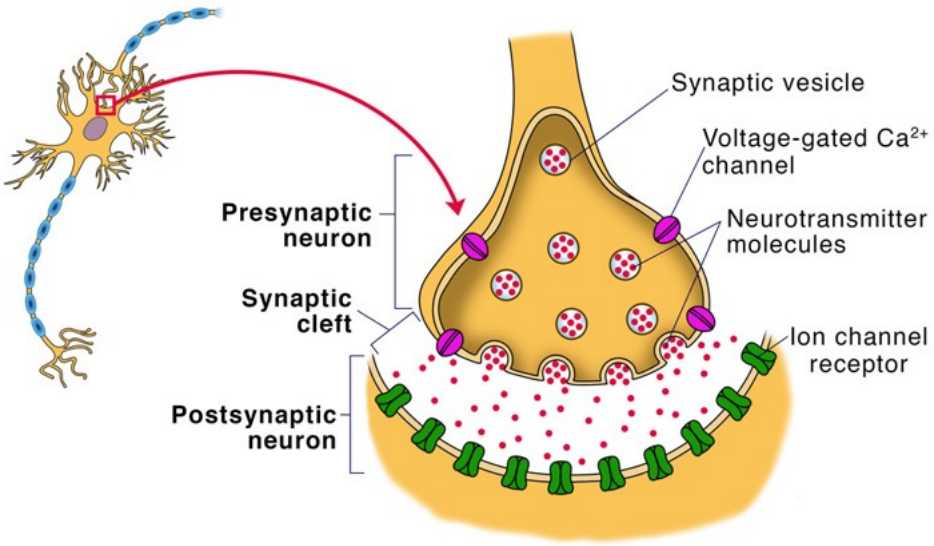

Fig. 2. The structure of a synapse. The synapse is an electrochemical connection between two neurons. It is composed of a presynaptic part, which is filled with synaptic vesicles containing neurotransmitters, a postsynaptic membrane harboring neurotransmitter receptors, and the synaptic cleft, the space between the two neurons.
Picture extracted from [online], URL: https://www.sciencefacts.net/synapse.html

Synaptic damage after stroke

Synapses are the basic structure underlying neuronal networks. The disappearance of synaptic activity is the first consequence of cerebral ischemia (Hofmeijer and Van Putten, 2012). As shown by an *in vivo* tracing technique, ischemic focal stroke causes axonal swelling and varicosity in different areas of the brain as early as 6h and up to four weeks after reperfusion (Q. Zhang et al., 2012). It also leads to dendritic spine length and density changes in the peri-infarct cortical area, which, interestingly, are spatially and temporally dynamic (Brown et al., 2008). Apart from the ultrastructural change in the peri-infarct area, the neuronal activity and blood flow also decrease in the remote brain area due to deafferentation originating at the lesion area, in a process called diaschisis (Gold and Lauritzen, 2002). Hydropic degeneration of axial dendrites and axodendritic synapses was found at the sites of diaschisis in an ultrastructural study of animals (Lee et al., 2020).

Numerous studies have investigated the underlying subcellular mechanisms of synaptic dysfunction after stroke, and several mechanisms can account for that: (i) presynaptic

failure. It was shown that hippocampal synaptic transmission failure after hypoxia *in vitro* was caused by presynaptic failure (Sun et al., 2002). Further investigation suggested that a decrease in synapsin1 phosphorylation might be the reason for this presynaptic failure (Bolay et al., 2002). A recent study has shown that synaptosome-associated protein 29 (SNAP29) expression is decreased both, in an *in vitro* OGD model and a middle cerebral artery occlusion animal model. SNAP29 knockdown was used to mimic SNAP29 expression reduction after stroke and it was observed by transmission electron microscope that the size of the readily releasable pool (RRP) located in the presynaptic site was decreased, however, the neuronal survival was not influenced. SNAP29 knockdown mice manifested impairment in the hippocampus-middle prefrontal cortex circuit and behavioral dysfunctions, indicating that SNAP29 can be implicated in the poststroke outcome through disruption of the presynaptic function (Yan et al., 2021). (ii) inhibition of voltage-gated calcium channels. Through voltage clamp experiments, it was shown that the inhibition of voltage-gated calcium channels due to increased intracellular concentration of calcium under hypoxic insult might be another mechanism of presynaptic failure (Hofmeijer and Van Putten, 2012). (iii) change of the spatial arrangement and number of synaptic vesicles (SV). In an *in vivo* ischemia experiment, the SV in the RRP from the active zone increased by 24%, and the inter-vesicle distance increased by 10% 15 min after reperfusion. Moreover, the number of SV dropped constantly until 7 days after stroke. (Nikonenko and Skibo, 2004). (iv) changes in the PSD. An *in vivo* ultrastructural study presented that PSDs were enlarged after transient ischemia in the hippocampal CA1 area and the dentate gyrus (Martone et al., 1999). (v) complement activation. Complement activation is an upstream mechanism of post-stroke inflammation. C3 activation is a critical step in the complement cascade, producing the C3a opsonins and activating the downstream membrane attack complex (MAC). It was demonstrated that opsonization of synapses by the complement caused the elimination of synapses by microglia phagocytosis, lasting for at least 30 days after stroke in reperfused and non-reperfused brains of C57bl/6 mice, and complement activation inhibition increased cognitive ability

(Alawieh et al., 2020). (vi) Cofilin rod formation. Cofilin is a protein that promotes the turnover of actin under physiological conditions. Pathological conditions, such as ATP depletion, could cause the formation of cofilin rods, containing cofilin and actin (Minamide et al., 2000). Demonstrated by real-time live cell imaging, immunostaining, and patch clamp studies, the formation of cofilin rod in peri-infarct surviving neurons and MCAO-reperfusion rat model after stroke jeopardized the dendritic mitochondrial function, synaptic structure, and function in cultured neurons (Shu et al., 2019).

Evidence of synaptic recovery after stroke

Early microscopic studies showed that after an ischemic insult, synapses are decreased in numbers till day 4, a turning point from where they start to recover until 1-12 weeks after ischemia (Ito et al., 2006). Recovery of the majority of dendritic spines was observed from 3 hours up to around 30 days after transient I/R *in vivo* experiments (Zhu et al., 2017). More strikingly, Vrselja and colleagues demonstrated that synaptic activity in pig brains could be restored *ex vivo* even 4 hours of postmortem interval (PMI), proving a previously underappreciated resilience of the brain for anoxic conditions (Vrselja et al., 2019). An interesting biophysical model of a tripartite synapse (anatomical and functional inter-relationship between pre- and post-synaptic compartments and surrounding astrocytes), calibrated with experimental data, could show that the critical step of synaptic failure under energy deprivation is the failure of Na^+/K^+-ATPase on astrocytes, and that through blocking voltage-gated Na^+ and K^+ channels, the synaptic pathological status can be reverted (Kalia et al., 2021).

Tools to study the synapsis: the synaptosome

Synaptosomes, firstly prepared in the late 1950s and validated in the 1960s, are isolated nerve endings widely used as a reliable model for investigating synaptic physiology (Evans, 2015). They contain the pre- and post-synaptic compartments and the synaptic cleft in between (Cotman and Taylor, 1972). They are membranous sacs comprised of the lipid bilayer, mitochondria, and synaptic contents (Picone et al., 2021). To isolate synaptosomes, after a mild disruption of the brain tissue and differential centrifugations,

discontinuous Ficoll/sucrose density gradients are used. Synaptosomes are functionally and structurally preserved (Ling and Abdel-Latif, 1968), and have been used for investigating synaptic anatomical structures, protein components, dynamics, and for the exploration of novel therapeutic agents of various neuronal diseases models over the years (Bai and Witzmann, 2007, Cisani et al., 2021, Hacioglu et al., 2021). Very recently, synaptosomes have been proposed as a delivery system of healthy mitochondria to neurons in neurodegenerative diseases (Picone et al., 2021).

Another way of brain communication and therapeutic delivery: Extracellular vesicles (EVs)

EVs are lipid bilayer particles secreted to the extracellular space from all types of cells, categorized into exosomes, microvesicles, and apoptotic bodies subtypes (Yáñez-Mó et al., 2015). These subtypes vary in size, subcellular origin, content, and intracellular trafficking. Exosomes are produced at the endocytic pathway. After extracellular materials are endocytosed and wrapped into early endosomes, through inward budding of the endosomal membrane, endosomes mature as intraluminal vesicles (ILVs) in the multivesicular bodies (MVBs) where they can then either be sorted into the lysosomal system to be degraded or fuse with the plasma membrane and release the ILVs which then are called exosomes to the extracellular space. The size of exosomes ranges from 30-150 nm. Microvesicles, whose diameter ranges from 100 nm to 1 μm, are EVs directly budded from the plasma membrane. Apoptotic bodies are products of apoptotic cells, formed by the budding of the plasma membrane and enclosing intact organelles, chromatin, and proteins. They have a relatively larger size ranging from 50 nm to 5000 nm (Doyle and Wang, 2019).

EVs were initially identified as a means of shedding unwanted intracellular materials (Johnstone et al., 1987). However, studies of recent years defined their roles in many physiological and pathological processes (Lo Cicero et al., 2015). Their cargo includes proteins, genetic material, lipids, and metabolites that can be taken up by the recipient cell eliciting a response (Van Niel et al., 2018). They are present in all kinds of body fluids, representing a good source of disease biomarkers as they reflect the state of the

cell of origin. But they are also very attractive therapeutic vehicles as they can be loaded with proteins, nucleic acid, lipids, and drugs and they can be delivered into the CNS from the bloodstream through the BBB, which is always a hurdle when it comes to transporting drugs into the CNS (Saint-Pol et al., 2020). For instance, catalase loaded in fluorescently labeled exosomes has been proved to be able to enter into recipient cells, neutralize ROS *in vitro* (PC12 neuronal cells) as well as in a model of Parkinson's disease (PD), leading to increased neuronal survival (Haney et al., 2015).

Materials and Methods

Animals

All animal experiments were approved by the local animal care committee (Behörde für Lebensmittelsicherheit und Veterinärwesen, project number: N45/2018, ORG_1055) and in accordance with the guidelines of the animal facility of the University Medical Center Hamburg-Eppendorf. C57BL/6 mice were used in all experiments.

Transient middle cerebral artery occlusion (tMCAO)

Transient focal ischemia was induced by intraluminal occlusion of the left middle cerebral artery as previously described in detail (Gelderblom et al., 2009) with minor changes. To exclude the protective effect of estrogen, all mice used were male (aged between 11-17 weeks). Briefly, the animals were anesthetized with isoflurane (1% to 2% v/v oxygen) and underwent analgesia (buprenorphine 0.03 mg/kg body weight). The surgery started after the pain reflex (paw withdrawal) disappeared. After the middle line incision on the neck, the left carotid artery branches were exposed and tMCAO was accomplished by first inserting the intraluminal filament (6-0 nylon) into the left external carotid artery and then inverting it into the internal carotid artery until reaching the middle cerebral artery. After 45 minutes of artery occlusion, the filament was removed to allow reperfusion. In the sham group, the arteries were exposed but no operation was performed.

Isolation of synaptosomes

Synaptosomes were isolated from fresh tissue. After harvesting the mouse brain, the cerebellum and brain stem were dissected and the ipsilateral hemisphere was placed in the homogenization buffer (1:10 w/v in 5mM HEPES pH=7.4 with 0.32 M sucrose with protease inhibitors (Sigma #11697498001)). The tissue was gently homogenized with a Dounce grinder with 15 up-and-down even strokes on ice. Then the sample was centrifuged at 4°C for 10 min at 1000 x g, the supernatant (S1) was collected and preserved on ice, and the pellet was resuspended with the same homogenization buffer and centrifuged again. The supernatant (S2) was collected, the pellet discarded, and the

supernatants from the two centrifugations (S1+S2) were combined, and then centrifuged at 4°C for 15 min at 12,000 x g. The resultant pellet was resuspended again in homogenization buffer and centrifuged at 4°C for 20 min at 12,000 x g to wash it. The resulting pellet (crude synaptosome fraction) was resuspended in 1 ml of 0.2 M sucrose in 5 mM HEPES buffer. Then the suspension was added to the top of a sucrose gradient (0.8 M, 1.0 M, 1.2 M in 5mM HEPES buffer pH=7.4) and ultracentrifuged at 4°C for 2 h at 82,600 x g (Beckman ultracentrifuge optima L-100 XP). After the centrifugation, the whitish band at the interface between 1.0 M and 1.2 M sucrose gradient was collected and resuspended in 10 ml of 0.2 M sucrose HEPES buffer and ultracentrifuged again at 4°C for 30 min at 26,000 x g. The resulting pellet, consisting of purified synaptosomes was resuspended in 4% paraformaldehyde (PFA) containing 2.5% glutaraldehyde for electron microscopy observation, or in 10 mM HEPES buffer pH=7.8 for mass spectrometry analysis, or in radioimmunoprecipitation assay (RIPA) buffer (50mM Tris base, 150mM NaCl, 1% NP40, 0.5% Na-Deoxycholate, 0.1% sodium dodecyl sulfate (SDS), 1mM phenylmethylsulfonyl fluoride (PMSF)) containing protease inhibitor for western blot analysis.

Electron microscopy

To check if the synaptosomes are correctly isolated, the pellet of synaptosomes fixed in 4% PFA containing 2.5% glutaraldehyde in PBS were first centrifuged and washed 3 times with PBS, then embedded in 3% agarose and cut into small slices. Osmification was performed on the slices to add more contrast to the samples. Afterwards, the samples were gradually dehydrated with ethanol and embedded in Epon resin (Carl Roth, Germany) for sectioning and trimmed smaller with Leica Ultra Cut to ultrathin sections (60 nm). Samples were analyzed using an EM902 transmission electron microscope (Zeiss, Germany) equipped with a CCD in lens 2K digital camera and running the ImageSP software (Tröndle, Moorenweis, Germany).

Electrophoresis and western blot

To characterize the synaptosome and check for synaptic markers enrichment (comparing

them with total homogenates), the protein concentrations were measured with Pierce BCA protein assay. Samples were then set up to a protein concentration of 1 µg/µL in Laemmly loading blue buffer 1x (60 mM Tris Base, 2% SDS, 10% glycerol, 0.05% bromophenol blue, 1.25% β-mercaptoethanol, pH6.8) and deionized H_2O. Samples were then denatured at 95°C for 5 min, and 9 µg of protein was loaded in a 12% acrylamide gel. Electrophoresis was performed at 100 mV in a Mini-PROTEAN Tetra cell (BIO-RAD). Proteins were then transferred onto nitrocellulose membranes (LI-COR #926-31092) in a wet chamber (Mini-PROTEAN II cell (BIO-RAD)) by using transfer buffer (25 mM Tris base, 192 mM glycine, 10% methanol). To assess for efficiency of transfer and to have a protein loading control, the membranes were then dyed with Revert Total Protein Stain Kit (LI-COR #926-11015) following the manufacturer's instruction and developed in an Odyssey® CLx Infrared Imaging System (LI-COR Biosciences). Subsequently, unspecific unions were blocked with Roti-Block buffer (ROTH #A151.2) 1x for 1 hour at room temperature. Primary antibodies were incubated at 4°C overnight on a shaking platform. For synaptosome characterization, the antibodies used were: mouse antibody against PSD95 (1:1000, Millipore #MABN68), mouse antibody against GM130 (1:1000; BD Biosciences #610822), rabbit antibody against Synapsin1 (1:1000; Synaptic Systems #163103), rabbit antibody against SNAP25 (1:2000; Cell Signaling #3926), and mouse antibody against Histone H1 (1:500; Millipore #MABE446). For verifying the proteomic datas a goat antibody against Cystatin C (1:1000; R&D #AF1238) was used. Afterwards, the membranes were washed with TBST buffer 1x (1:10; 100mM Tris Base, 140mM NaCl, pH7.4, 0.1% Tween-20) for 5 min 3 times and then incubated with the appropriated secondary antibody (anti-Mouse (1:1000; Cell Signaling #7076), anti-Rabbit (1:1000; Cell Signaling #7074), anti-Goat (1:1000; Promega #V805A)) for 1 hour at room temperature while shaking. After intensive washings with TBST buffer, the membranes were developed with SuperSignal West Pico PLUS chemiluminescent substrate (Thermo Scientific #34577) or SuperSignal West Femto maximum sensitivity substrate (Thermo Scientific #34095), and then the chemiluminescence signals on the membranes were visualized and pictured with either

a ChemiDoc imaging system (BIO-RAD) or an Azure 400 visible fluorescent western system (Biozym). The protein bands' signal intensities were analyzed with Image Studio software (LI-COR).

Mass spectrometry

For proteomic analysis, the concentrations of synaptosome samples were measured with the Pierce BCA Protein Assay Kit (Thermo Fisher #23225) following the manufacturer's instructions and then diluted to 1 µg/µL. 20 µg of each sample was used for tryptic digestion. Disulfide bonds were reduced, using 10mM DTT for 30 minutes at 60°C. Alkylation was achieved with 20 mM iodoacetamide (IAA) for 30 minutes at 37°C in the dark. Tryptic digestion was performed at a trypsin: protein ratio of 1: 100 overnight at 37°C and stopped by adding 1% Formic acid (FA). The sample was dried in a vacuum concentrator (SpeedVac SC110 Savant, (Thermo Fisher Scientific, Bremen, Germany)) and stored at -80°c until further usage. Directly prior to LC-MS analysis, samples were resolved in 0.1 % FA to a final concentration of 1 µg/µl. 1 µg of tryptic peptides was injected into a UPLC (nano Ultra-Performance Liquid Chromatography, nanoAcquity system, Waters, Milford, MA, USA). Chromatographic separation of peptides was achieved with a two-buffer system (buffer A: 0.1% FA in water, buffer B: 0.1% FA in ACN). Attached to the UPLC was a peptide trap (180 µm × 20 mm, 100 Å pore size, 5 µm particle size, Symmetry C18, Waters) for online desalting and purification followed by a 25-cm C18 reversed-phase column (75 µm × 200 mm, 130 Å pore size, 1.7 µm particle size, Peptide BEH C18, Waters). Peptides were separated using an 80 min gradient with linearly increasing ACN concentration from 2% to 30% ACN in 65 minutes. The eluting peptides were analyzed on a Quadrupole Orbitrap hybrid mass spectrometer (QExactive, Thermo Fisher Scientific). Here, the ions responsible for the 12 highest signal intensities per precursor scan (1 × 106 ions, 70,000 Resolution, 240ms fill time) were analyzed by MS/MS (higher-energy collisional dissociation (HCD) at 25 normalized collision energy (1 × 105 ions, 17,500 Resolution, 50 ms fill time) in a range of 400–1,200 m/z. A dynamic precursor exclusion of 20 s was used.

LC-MS/MS data were searched with the Sequest algorithm integrated into the Proteome Discoverer software (v 2.41.15, Thermo Fisher Scientific) against a reviewed murine Swissprot database, obtained in April 2020, containing 20365 entries. Carbamidomethylation was set as a fixed modification for cysteine residues and the oxidation of methionine, and pyro-glutamate formation at glutamine residues at the peptide N-terminus, as well as acetylation of the protein N-terminus were allowed as variable modifications. A maximum number of 2 missing tryptic cleavages was set. Peptides between 6 and 144 amino acids were considered. A strict cutoff (false discovery rate (FDR) <0.01) was set for peptide and protein identification. Protein quantification was carried out, using the Minora Algorithm, implemented in Proteome Discoverer.

In vitro experiments

Primary neuronal cell culture

For hippocampal neurons, C57BL/6 pups at postnatal day 1-2 (P1-2) were used. After decapitation, the pups' brains were dissected and the meninges were removed with caution. The hemispheres were flipped over with a fine tweezer to expose the hippocampi, which were taken and placed in ice-cold PBS/10 mM glucose. After hippocampi collection, the PBS/10 mM glucose was removed carefully and changed to 5mL digestion solution (PBS/10 mM glucose, 0.5 mg/mL papain(Sigma #P4762-100MG) and 20 µg/mL DNase (Sigma #DN25-10MG)), and the preparations were placed in a 37°C shaking water bath for 30 min. Afterwards, the digestion solution was removed, and the hippocampi were washed with a plating medium(70% (v/v) MEM (Gibco #51200-046), PBS/20mM glucose, and 10% (v/v) horse serum (Gibco #16050-130)) 4 times and subsequently resuspended in 1 mL plating medium. 20 µL of cell suspension was combined with 20 µL Trypan Blue (Sigma #T8154-100ML), and cell number was counted with a Countess® II cytometer (Thermo Fisher Scientific #AMQAX1000). 70,000 cells/well were plated in 24-well plates containing poly-L-lysine (Sigma #P9155-5MG) coated 13 mm diameter coverslips with (500ul/well) plating medium. The coverslips were coated with poly-L-lysine at 37°C for 2-3 hours in

advance and then washed three times with PBS. 3 to 4 h later, the plating medium was changed to 1 mL/well maintenance medium (Neurobasal A (Gibco #10888-022) containing 0,1 % Gentamicin (Thermo Fisher #15750-060), 1x Glutamax (Thermo Fisher #35050-038) and 2% B27 serum (Gibco #17504-044)). Half of the maintenance medium was changed every 3-4 days. Primary neurons were cultured for 14 days for them to establish the mature synaptic network.

Oxygen-glucose deprivation (OGD)

OGD on primary neuronal cell cultures was performed on day *in vitro* (DIV) 14 as previously described with some modifications (Lossi and Merighi, 2014). In brief, cells were briefly rinsed in 1ml of pre-warmed OGD medium (Neurobasal A medium without glucose (Gibco #A24775-01) containing 0,1 % Gentamicin, 1x Glutamax, and 2 % B27 serum) twice to deplete glucose from intracellular storage, and then exchange the medium for pre-warmed OGD medium (1ml/well). Afterwards, the 24-well plate without lid was put into an anaerobic chamber (Modulator incubator chamber, Billups-Rothenberg #5352414) under sterile conditions, closed, and flushed with a gas mixture of 95% N_2, 5% CO_2 for 5 min at a flow rate of 4-6 L/min to yield an N_2-enriched atmosphere before complete closure. The anaerobic chamber was placed back into the incubator at 37°C for 20 min (Z. Zhang et al., 2020). After OGD exposure, the plate was removed from the anaerobic chamber and the OGD media was changed back to the normal maintenance medium. Control neurons were treated in parallel as with the OGD coverslips, except being washed and maintained in normal culture medium and incubated at normal conditions with 5% CO_2 at 37°C.

Cystatin C treatment

The human urine recombinant Cystatin C (Millipore Sigma #240896-50UG), when referred to, was added at a concentration of 0.15 µM into the maintenance medium immediately after OGD. Control groups were added with the same volume of solvent (100 mM sodium acetate buffer, pH 4.5) to eliminate its effect. Four conditions were set up at this stage: normoxia + solvent, normoxia + Cystatin C (CysC), OGD + solvent and

OGD + CysC.

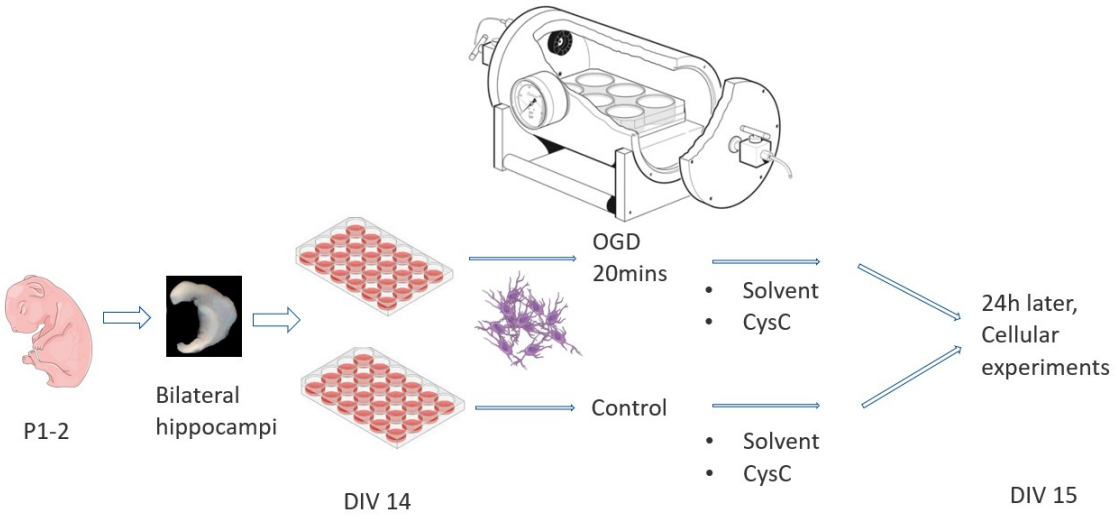

Fig. 3. Workflow of primary neuronal cell culture and OGD. The hippocampal neurons isolated from P1-2 pups were seeded on coverslips in two 24-well cell plates. After maturation for 14 days in the maintenance cell medium, the medium in one plate was changed to a D-glucose medium and placed in the anaerobic chamber for 20 min at 37°C. At the same time, the medium in the other plate, as control group, was changed to the maintenance medium and maintained at normal conditions with 5% CO_2 at 37°C for 20 min. Afterwards, the medium in the two plates was changed back to their original maintenance medium and incubated at normal conditions with 5% CO_2 at 37°C. Viability assays or cell fixation for immunocytochemistry were performed 24h afterwards.

Addition of CysC loaded in EVs

EVs were isolated from mice brains and loaded (or not, as a control) with CysC at a concentration of 1.28 ng/µl by our collaborators in the USA (professor Efrat Levy, Department of Biochemistry and Molecular Pharmacology, NYU Langone Health, New York). 4.8* 10^9 particles/µl of EVs were added to the primary neuronal cell culture after the OGD treatment. Four conditions were set up at this stage: normoxia + empty EVs (eEVs), normoxia + CysC-loaded EVs (cEVs), OGD + eEVs and OGD + cEVs.

Cell viability assay

LDH assay

The CyQUANT™ LDH Cytotoxicity Assay (Thermo Fisher #C20300) was used to detect cytotoxicity 24 hours after OGD according to the manufacturer's manual. As a positive control (100% of cell death), 10X Lysis buffer was diluted with maintenance medium to 1X and added to the designed wells, and incubated for 45 min. For the test,

100 µl of cell medium from each condition, together with the positive control were evenly divided into two wells in a 96-well plate (with 2-3 replicates per group). Afterwards, 50 µl of Mixture Solution was added to each well and incubated for 30 min at room temperature in the dark. Wells (without cells) filled with medium containing either only solvent or only CysC were used as background control. After incubation, 50 µl of Stop solution was added and the absorbance was detected at 470nm in a BioTek microplate reader.

MTT assay

The CellTiter 96® Non-Radioactive Cell Proliferation Assay (MTT) (Promega #G4000) was used to check cell viability 24h after OGD treatment following the manufacturer's instruction. Briefly, cells were first incubated with Dye solution (10% v/v added to the cell maintenance medium) for 4 hours at 37°C, to allow the tetrazolium salt in the Dye solution to be converted into a formazan product by the living cells. Then the Solubilization solution in the same amount as the medium was added to the culture wells to solubilize the formazan product at room temperature for at least 1 hour. The solution containing only the formazan product was transferred to a new 24-well plate. Wells filled with medium containing only solvent were used as background control. Absorbance was recorded at 570nm using a BioTek microplate reader. 2-3 replicates were used in each group.

Immunocytochemistry

The immunocytochemical analysis was performed as previously described with minor alterations (Brenna et al., 2020). Shortly, cells plated on coverslips were fixed on day 15 after plating with 4% PFA for 10-15 min at room temperature, washed three times with PBS for 5 min, and permeabilized with 0.5% saponin in PBS for 10 min at room temperature. Afterwards, a buffer to block unspecific unions containing 1% BSA in PBS-Tween (0.1%) was added for 30 min. Without washes in between, primary antibodies diluted in 1% BSA in PBS were added and incubated at 4°C overnight in a wet chamber. The next day, samples were washed three times with PBS for 5 min and

incubated with secondary antibodies diluted in 1% BSA in PBS for 30 min at room temperature. After washing three times with PBS for 5 min, coverslips were mounted with DAPI Fluoromount-G mounting medium (Southern Biotech #0100-20) and air-dried overnight. Nail polish was used to seal the coverslip edge. The primary antibodies used were: goat antibody against MAP2 (S-15) (1:100; Santa Cruz #sc-12012) and rabbit antibody against Synapsin1 (1:500; Synaptic Systems #163103). The secondary antibodies used include: anti-goat 555 (1:500; Thermo Fisher #A21432) and anti-rabbit 488 (1:500; Thermo Fisher #AF21206).

Confocal microscopy

To quantify synaptic density, images were taken with a Leica TSC SP8 confocal microscopy. A mean of 10 neurons (between 7~13) were chosen per coverslip, and 2-3 coverslips were checked per condition per experiment, so a total of 20-25 neurons per condition per experiment were imaged. The neurons were always observed with the 63x objective. For the 3D images, the z-stacks were set up at 0.3 µm. Images were taken with a resolution of 1024 x 1024 pixels with a 1X digital zoom throughout all experiments. The starting and ending points of the z-series are determined by the starting and ending points of neuronal dendritic spatial distribution on the z-axis. Only neurons that were clearly isolated but also not far away from other neurons and with a dendritic length of 80-100% width or height of the picture frame (90 x 90 µm) were chosen. For synaptic quantification, the z-stacks were reconstructed with the Imaris software (Bitplane 7.4.2). Within the surpass module, the optimized settings used to reconstruct the dendrites and synapses were fixed for every experiment.

In vivo experiments

Intracerebroventricular injection of EVs loaded with/without CysC

Mice were subjected to tMCAO as described above, and 6 h after artery occlusion, 2µl of EVs from group A or B (we were blinded about which group was loaded with Cystatin C) were injected into the ipsilateral ventricle (n=6 per group) with a stereotactic device (Stoelting #51730D). The injection coordinates used were 1.1 mm

lateral, 0.5 mm posterior, and 2.3 mm ventral to the skull bregma. In total 11 mice brains, 6 mice in group A and 5 mice in group B, were used for immunofluorescence analysis. Brains were isolated and processed with TTC staining as described below.

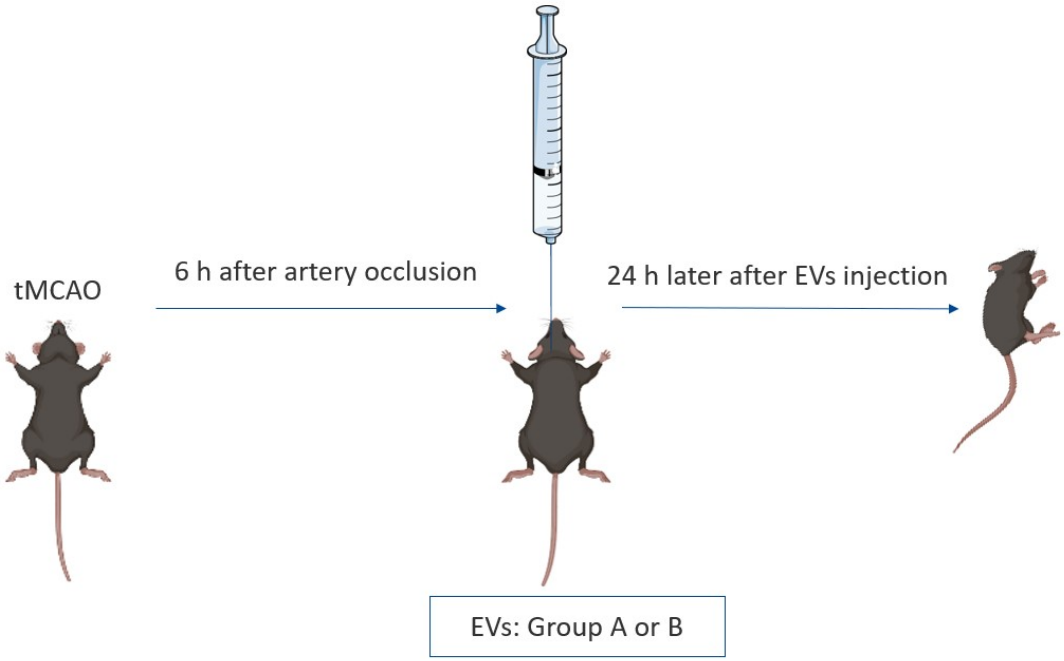

Fig. 4. Flow chart showing the intracerebroventricular injection of EVs on tMCAO mice. The artery occlusion time was recorded for each tMCAO mouse. 6h later, the frontal skin was cut and 2 μl of EVs were injected into the left lateral ventricle slowly at the point 1.1 mm lateral, 0.5 mm posterior, and 2.3 mm ventral to the skull bregma. 24h after EVs injection, the mice were sacrificed and their brains were harvested for further experiments.

TTC staining

2,3,5-Triphenyltetrazoliumchlorid (TTC) solution was used to check the stroke area of the brains, as colorless TTC is converted by the mitochondrial succinate dehydrogenase of live cells into formazan, turning viable brain tissue into red, while the unviable tissue remains white. In short, mice brains were sliced rostro-caudally into serial 1-mm-thick slices, then the whole set of brain slices was incubated in the TTC solution in a 60mm petri dish at room temperature for 20 min at room temperature. Brain slices were scanned and the stroke area was calculated with Image J software (National Institute of Health).

Immunofluorescence

After TTC staining, brain tissues were fixed with 4% PFA at 4°C for 24h, rinsed in ice-cold PBS, and embedded in paraffin in a Modular Tissue Embedding Center (Leica #EG1150H). Paraffin-embedded sections were cut at 5 µm with a microtome and then affixed to Superfrost microscope slides (VWR #631-0108). After drying at 37°C overnight, slides were deparaffinized and boiled for 20 min in citrate buffer (0.1 M Sodium Citrate and 0.1 M Citric acid in distilled H_2O) for antigen retrieval. After PBS washings, samples were incubated with 5% normal rabbit serum (Vector laboratory #S-5000) in PBS-0.2% Tween-100 (PBST) for 1 h at room temperature to block unspecific unions. Afterwards, the sections were incubated with primary antibodies diluted in 5% normal rabbit serum in PBS at 4°C overnight in a wet chamber. The next day, the slides were recovered to room temperature for 30 min and after PBS washes (5 min X 4 times), incubated with secondary antibodies diluted in 5% normal rabbit serum in PBS for 45 min at room temperature in the darkness. The slices were mounted with DAPI Fluoromount-G mounting medium (Southern Biotech #0100-20) sealed with nail polish, and let to air-dry in a dark chamber.

Primary antibodies used were: NeuN (1:2500, EMD Millipore #ABN91), GFAP (1:100, Invitrogen #13-0300). Secondary antibody used included: anti-chicken AF647 (1:500; Thermo Fisher #A21449), anti-rat AF555 (1:500; Abcam #ab150154). Anti-Isolectin GS-IB4, Alexa Fluor 488 (Invitrogen #121411) antibody was applied with the secondary antibodies.

Microscopy

For the whole brain tissue, immunofluorescence imaging was conducted with an Echo microscopy (Zeiss) with a 10x objective.

Statistical analysis

For MS statistical analysis each experiment was handled separately. Protein abundance values were log2 transformed and median normalized across columns to compensate for injection amount differences. Statistical testing was carried out, using the Perseus software (Max Plank Institute for Biochemistry, Version 1.5.8.5). For the identification

of differences between sham and stroke samples, Student's t-testing was applied (p-value <0.05, Foldchange difference > 1.5). Visualization of t-test results and abundance distributions across groups was performed in PRISM (GraphPad, Version 5). GraphPad Prism 9 software was used to analyze the data from western blot, cellular viability and cytotoxicity, and immunocytochemistry experiments. Student's t-test or Mann-Whitney U test were used to compare the difference between groups, and statistical difference was considered when *$p < 0.05$, **$p < 0.001$, ***$p < 0.0001$. Values are described as mean ± SEM. The exact p values are given in the text.

Results

Characterization of synaptosomes

Over several decades, synaptosome isolation has been refined and with the recent breakthroughs in techniques applied to synaptic proteome studies (i.e. mass spectrometry), a comprehensive understanding of synaptic proteins network has been achieved (Bai and Witzmann, 2007). To characterize our sample by western blot we used several known pre- and post-synaptic markers such as PSD95, SNAP25, and synapsin1 (Figure 5A). PSD95 is a protein located predominantly in the PSD and has been widely used as a postsynaptic marker (Sampedro et al., 1981). The synaptosomal-associated protein 25 (SNAP25) is present on the presynaptic membrane and is a member of target-SNAP proteins (t-SNAREs) which participate in the recycling of SVs and help in their docking and fusion with the pre-synaptic membrane (Walch-Solimena et al., 1995). Synapsin1 is also a presynaptic protein located mainly on the SV membrane, which helps in the docking between SVs and the presynaptic membrane (Hirokawa et al., 1989). As a negative control, to test the purity of the synaptosome enriched fraction, we used the cis-Golgi matrix protein GM130 (Nakamura et al., 1995), and the nucleus marker Histone H1 (Hergeth and Schneider, 2015). As shown in Figure 5 A, the three synaptic markers are enriched in the synaptosome fraction (SN) compared to total homogenate (TH), yet the GM130 and Histone H1 are absent from the fraction, proving the suitability of our isolation technique. Electron microscopy (EM) can provide high resolution in the range of the nanometer and it is the gold standard for synaptic structural analysis (Borges-Merjane et al., 2020). In Figure 5(B), it can be observed several putative synaptosome structures characterized by presynaptic terminals filled with SVs and the layer of the postsynaptic density, indicating that our synaptosome fraction is preserved.

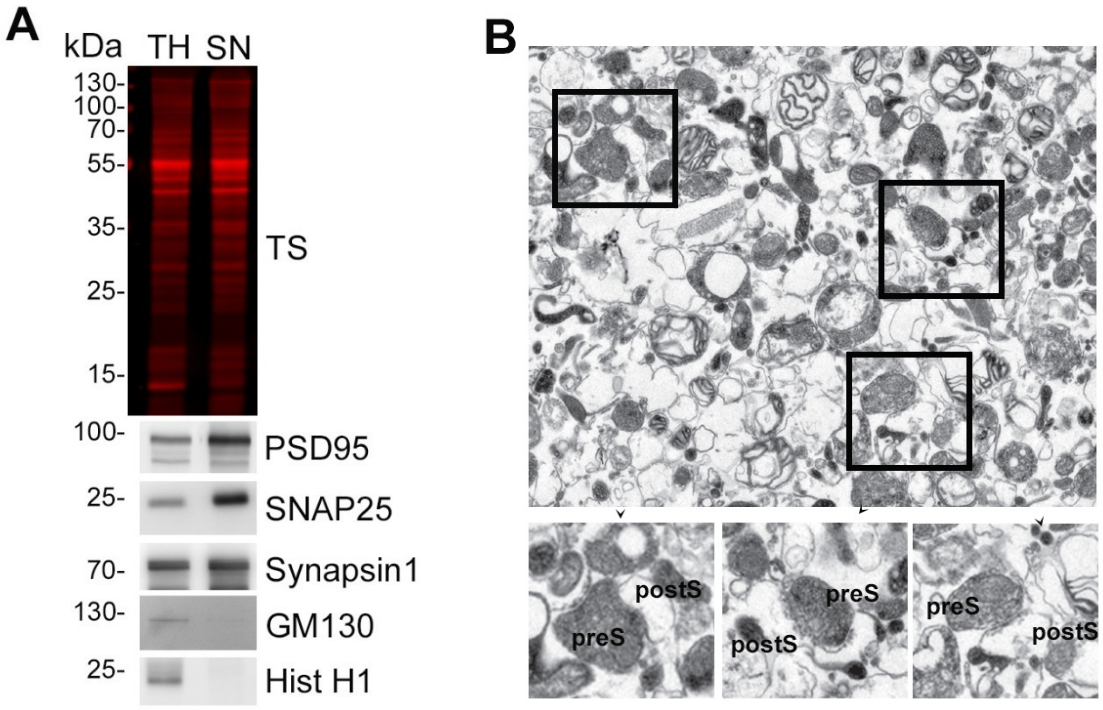

Fig.5. Characterization of synaptosomes by western blot and electron microscopy. (A). The synaptosome (SN) enriched fraction was compared to a brain total homogenate (TH), TS is the total protein stain showing that the same amount of proteins was loaded in each lane. The SN fraction is enriched in PSD95, Synapsin1, and SNAP25 when compared to TH. The SN fraction lacks GM130 and Histone H1 (Hist H1), indicating the purity of synaptosome isolation. (B). Electron microscopy picture showing multiple typical SN isolated structures (some highlighted in the squares) with their magnified version below. The presynaptic compartments are full of synaptic vesicles and the postsynaptic structures are marked by the postsynaptic density.

To assess the difference in synaptosome proteomes between sham and stroke groups over time, mice were subjected to tMCAO surgery for 45 min, and after 24h (n=4 per group), 4d (n=5 per group) and 7d (n=5 per group) of reperfusion, mice were sacrificed and synaptosomes were isolated from their ipsilateral hemispheres (cerebellum and pons were removed). Quantitative mass spectrometric proteome analysis was performed to detect the map of proteins in the two groups. More than 2000 proteins were identified at each time point, 79 proteins at 24h (54 upregulated), 92 proteins at 4d (24 upregulated), and 155 proteins at 7d (66 upregulated) were found differentially expressed. Only proteins identified in at least three out of four or five animals in one group were used for further analysis. For functional enrichment (GO terms) we found

that at 24h, Cellular response to stimulus (GO: 0051716) and Cellular process (GO: 0009987) were the most significant ones. Using the same data set, at 4d after stroke, upregulated proteins are enriched in bioprocess of regulation of cell death (GO: 0010941), negative regulation of glycoprotein metabolic process (GO: 1903019), and positive regulation of proteolysis (GO: 0045862). At 7d after stroke, with the same parameter setting, upregulated proteins are enriched in the bioprocess of cellular process (GO: 0009987), regulation of biological quality (GO: 0065008), and protein metabolic process (GO: 0019538). Figure 6 A shows the heat maps, the volcano plots, and the protein functional interactions of differentially expressed proteins at the 3 time points. From the protein list, we found that Cystatin C (CysC), the cysteine protease inhibitor, was significantly upregulated 4d after I/R compared to the sham group (fold change $\geq$ 1.5, $p < 0.05$; Fig 6B). When CysC was checked at 24h after I/R, it was found not detectable at all in shams and upregulated in two out of 4 stroke animals. Whereas at 7 days after I/R, the expression level of CysC was found not significantly different between the two groups.

Cystatin C is encoded by the CST3 gene in humans and is ubiquitously expressed in all nucleated cells (Mussap and Plebani, 2004). It is a cysteine protease inhibitor and has already been suggested as being protective towards ischemic insult and neurodegenerative processes, although the mechanism whereby they exert this protection is not elucidated (B. Yang et al., 2020, Gauthier et al., 2011). As our aim for the present study was to find inner mechanisms of neuronal survival/regeneration, we decided to focus on CysC for the next experiments.

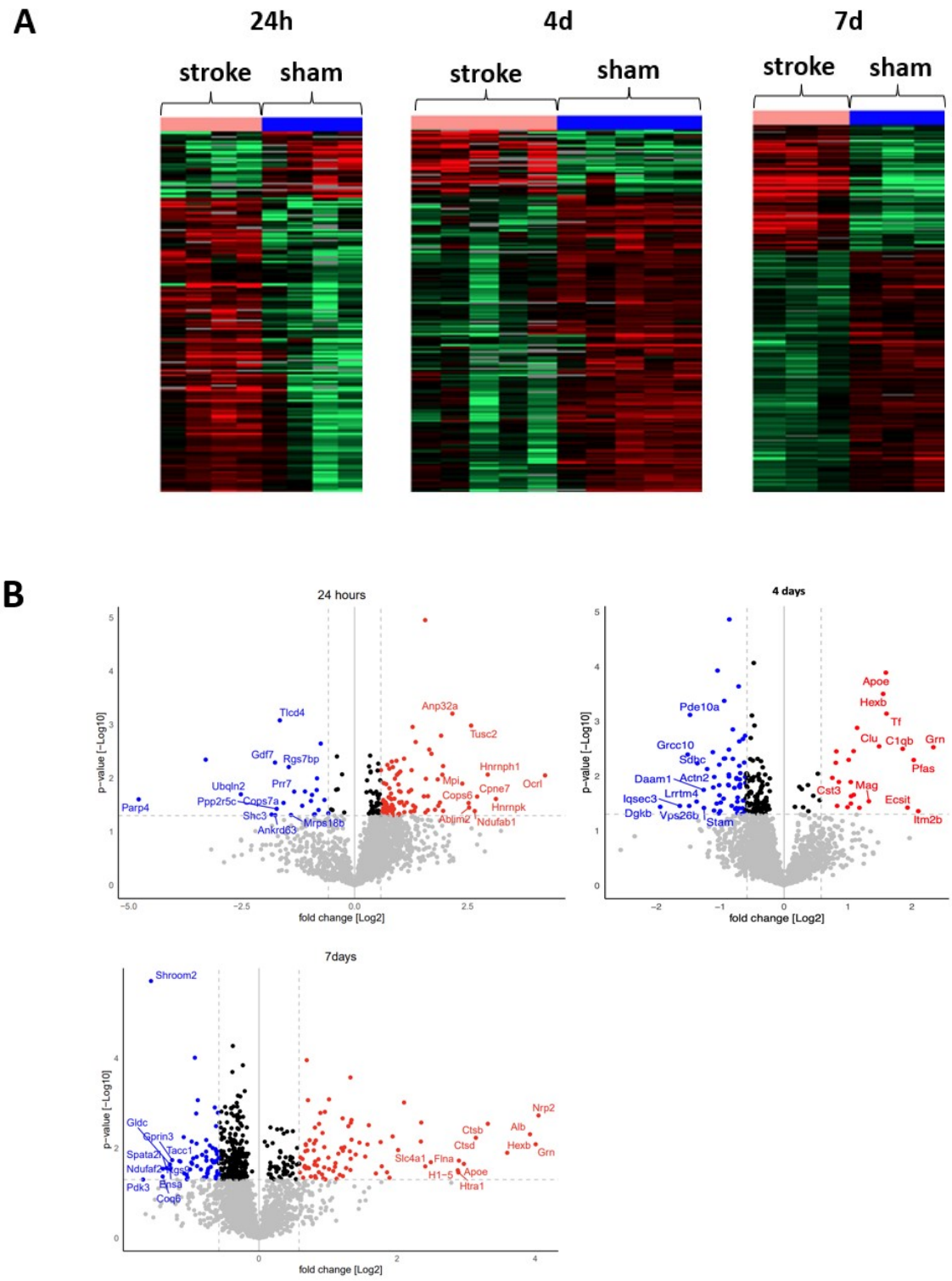
A
24h
4d
7d
stroke
sham
stroke
sham
stroke
sham
B
24 hours
4 days
7days
p-value [−Log10]
fold change [Log2]
Tlcd4
Gdf7
Rgs7bp
Ubqln2
Prr7
Ppp2r5c
Cops7a
Parp4
Shc3
Mrps18b
Ankrd63
Anp32a
Tusc2
Hnrnph1
Mpl
Ocrl
Cpne7
Cops6
Hnrnpk
Ablim2
Ndufab1
Pde10a
Grcc10
Sdhc
Daam1
Actn2
Iqsec3
Lrrtm4
Dgkb
Vps26b
Stam
Apoe
Hexb
Tf
Clu
C1qb
Grn
Pfas
Cst3
Mag
Ecsit
Itm2b
Shroom2
Gldc
Sprin3
Tacc1
Spata2l
Ndufaf2
Pdk3
Ens1
Coq6
Nrp2
Ctsb
Alb
Ctsd
Hexb
Grn
Slc4a1
Flna
H1−5
Apoe
Htra1

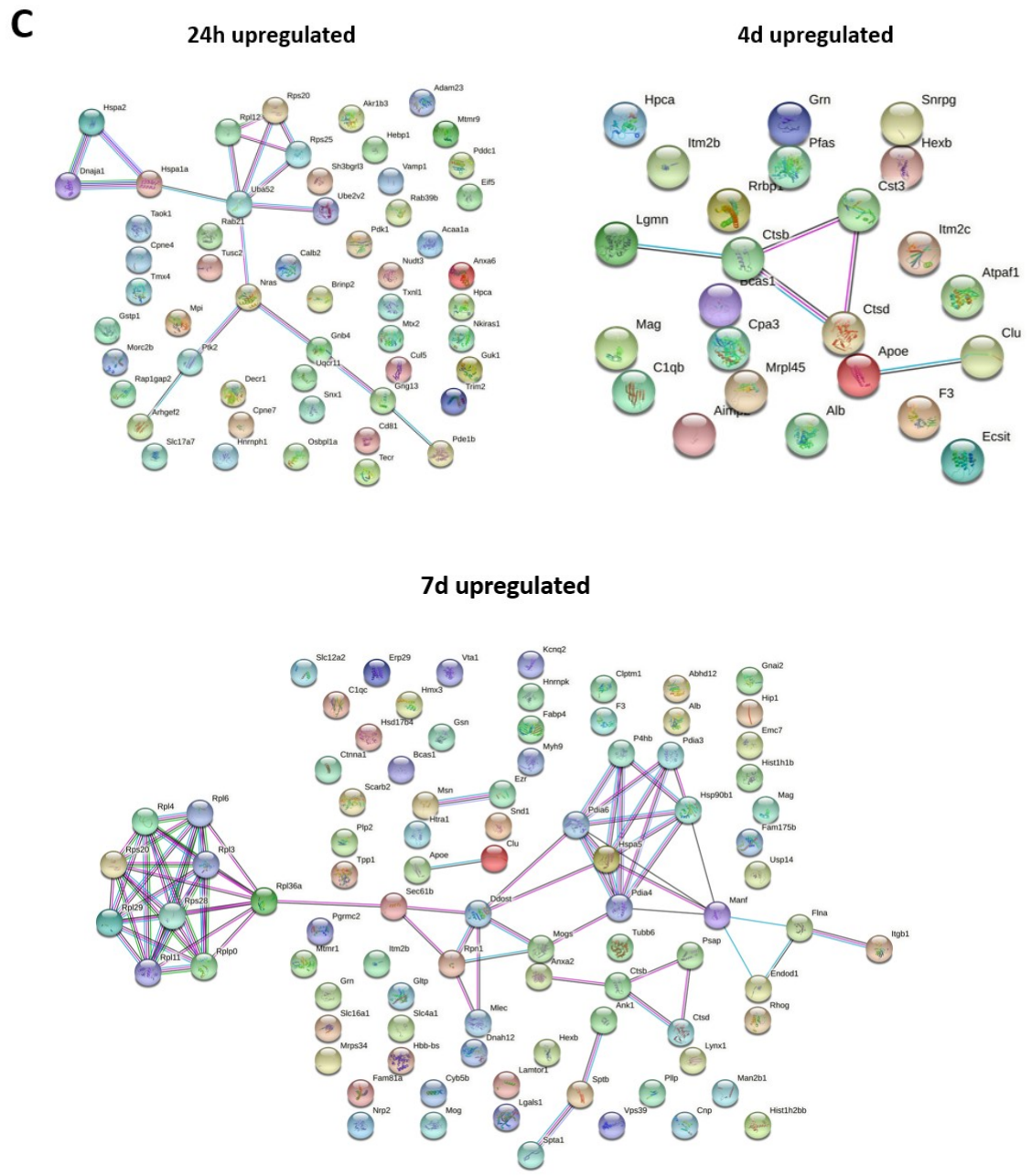

Fig.6. Mass spectrometry and STRING analysis results from synaptosomes at different time points after reperfusion. (A). Heat maps of proteins identified by proteomics that were significantly differentially expressed in stroke compared to sham groups at 24h (n=4), 4d (n=5), and 7d (n=3) after stroke. (B). Volcano plot showing the significantly upregulated (red dot) and downregulated proteins (blue dot) in stroke groups compared to the sham groups (|fold change| > 1.5, $p < 0.05$). The 10 most upregulated and downregulated proteins along with CysC are named at each time point. At 24h, CysC was screened out in further analysis as it was only found in two stroke animals. At 4d after stroke, its expression was significantly upregulated in the stroke group and tended to drop back to the same level as it is in the sham group at 7 days. (C). The STRING protein interaction analysis graph shows the possible functional and physical connections between the significantly upregulated proteins in the stroke group at different time points. The interaction score was set to high confidence (0.7) and no text-mining.

To confirm the results of CysC enrichment at 4 days after tMCAO (and partially at 24h) obtained by quantitative mass spectrometry, we performed western blot analysis. As shown in Figure 7, both, at 24h and 4 days after tMCAO a significant increase in CysC is observed (p=0.0286 and p=0.0159, respectively), whereas the difference disappears at 7 days. Interestingly, a decrease of the synaptic markers SNAP25 and PSD95 was also observed at 24h probably indicating the loss of synapsis at that time point (both p=0.0286). This difference is seen neither at 4 nor 7 days after stroke.

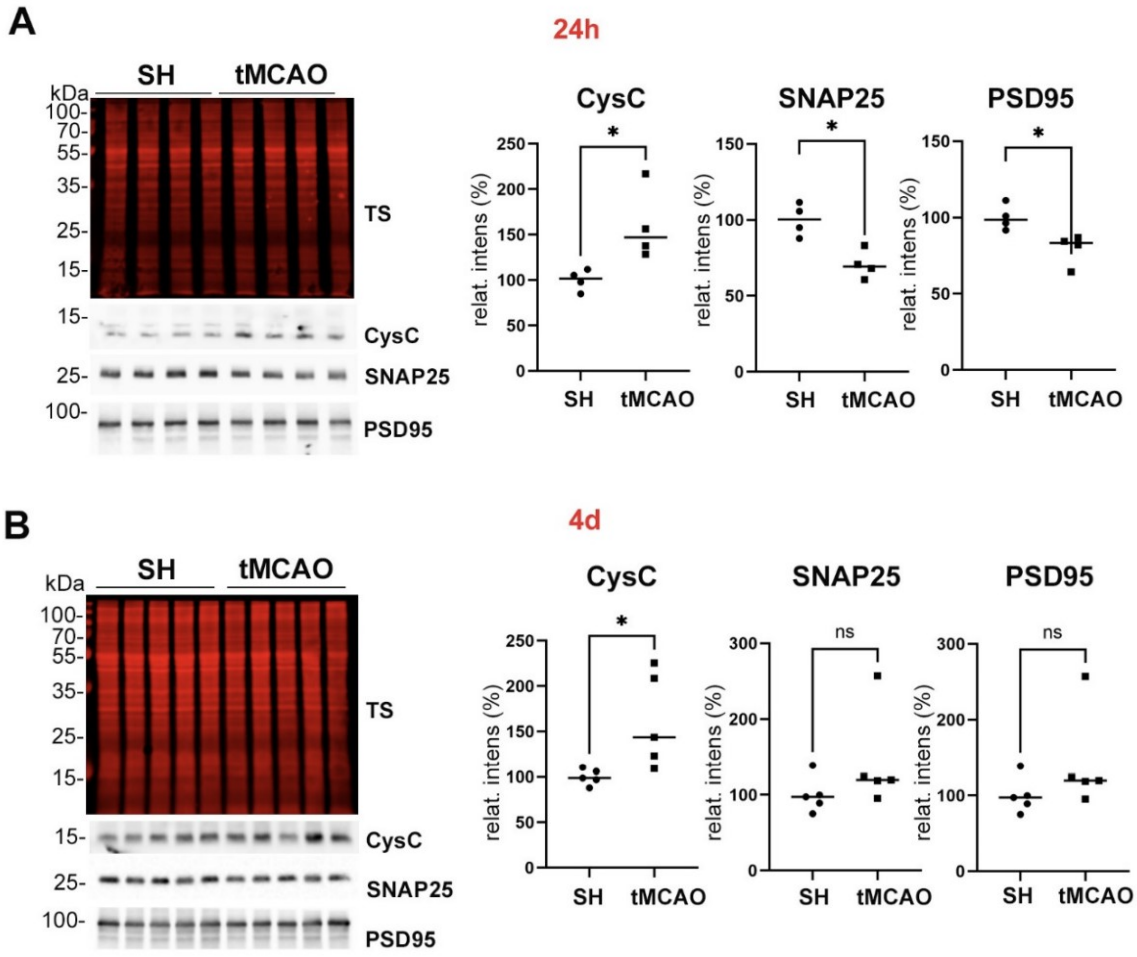

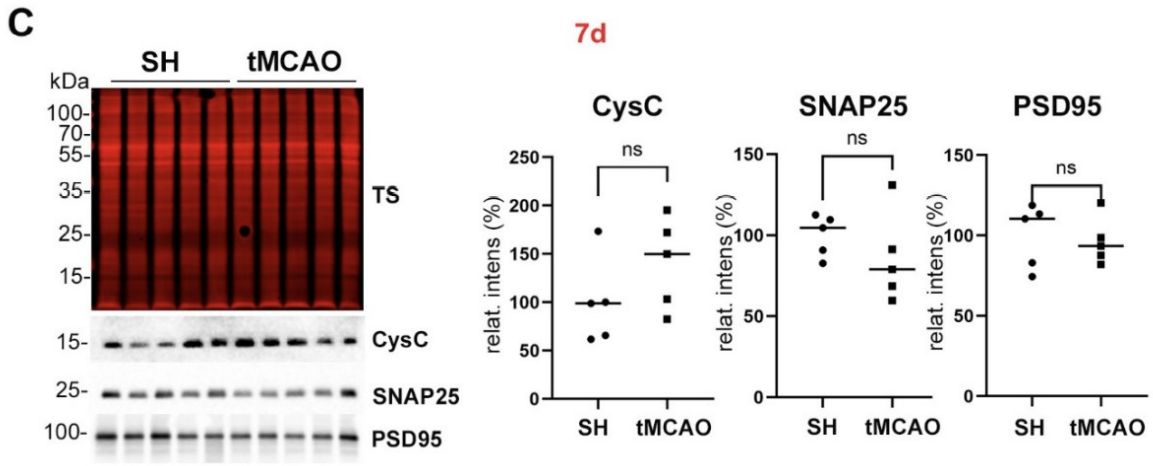

Fig.7 CysC is enriched in synaptosomes isolated from mouse brains at 24h and 4 days after tMCAO. (A) Western blot analysis of synaptosomes isolated from the ipsilateral brain hemisphere of mice 24h after tMCAO and reperfusion compared to shams (SH) (n=4 each group). The total staining (TS) shows equal protein loading. In the tMCAO group, two synaptic proteins, PSD95 and SNAP25 were significantly reduced whereas CysC was significantly upregulated (*p<0.05) as shown in the quantifications (on the right). (B) Same western blot analysis as in (A) but from synaptosomes isolated 4 days after tMCAO/reperfusion (n=5 each group). Total staining (TS) shows equal loading of protein. As in A, CysC is still significantly increased (*p<0.05) in tMCAO synaptosomes whereas PSD95 and SNAP25 do not show any difference between tMCAO and sham samples (ns, not significant) as shown in the quantifications (right panel). (C) Same analysis as in (A) and (B) but from synaptosomes isolated at 7 days after tMCAO/reperfusion and shams (n=5 each group). Here, no significant differences were observed for neither PSD95, SNAP25, nor CysC as shown in the quantifications in the right panel (ns, not significant).

In vitro experiments results

Neurons are still viable 20 min after OGD treatment but synapses are affected

Once we had confirmed that CysC was increased at 24h and 4 days after I/R in mice, we asked ourselves if the increase of CysC in the synaptosomes could be an inner mechanism of synaptic protection against the ischemic damage, as synapses are among the first targets in this condition. We then set up *in vitro* experiments to assess if, in the penumbra area, external treatment of CysC could be a mechanism of synaptic preservation.

To model the ischemic damage at the penumbra, we chose 20 min of OGD treatment as it has been shown that this is enough to cause synaptic damage. (Z. Zhang et al., 2020). To assess neuronal cytotoxicity we performed an LDH assay. Four groups were

established: (a) normoxia, where cells did not undergo OGD; (b) normoxia with CysC, to exclude any aberrant effect of CysC; (c) OGD-treatment; and (d) OGD with CysC. As a positive control, lysed neurons (100% cytotoxicity) were used. As shown in Figure 8(A), no significant differences in cytotoxicity were observed between OGD and normoxia groups, or between OGD and OGD with CysC group, meaning that 20 min of OGD treatment was only doing neglectable harm to the neurons and the addition of CysC did not have any effect. The comparison between the normoxia condition with CysC to normoxia alone condition indicated that CysC addition to the normal cell culture did not lead to any collateral effect. To assess neuronal viability as a complementary assay, we performed an MTT assay. Figure 8B shows that 20 min of OGD treatment did no alter significantly neuronal viability and that CysC did not have any substantial effect neither in normoxia condition nor after OGD. Thus, by two complementary methods, we could show that viability of neurons 20 min after OGD treatment was preserved.

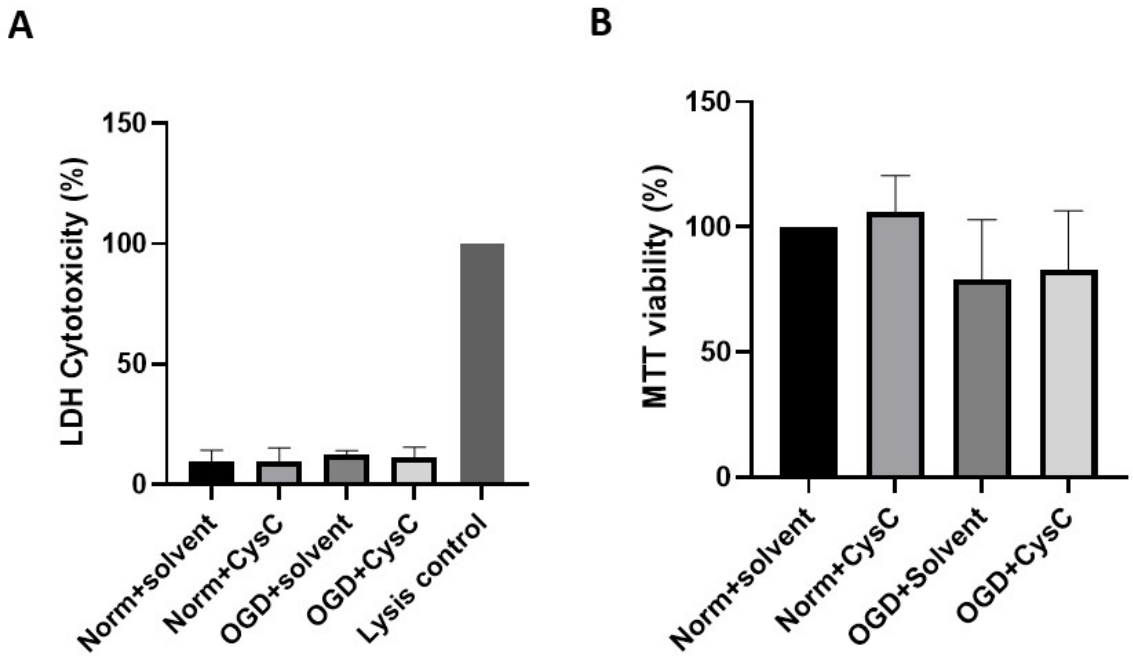

Fig.8. **No decrease in neuronal survival is observed 20 min after OGD treatment.** (A) LDH assay measured 24h after 20 min of OGD and normoxia treatment in neuronal cultures. CysC was added right after the OGD treatment in both conditions. The results are normalized with the maximal lysis control group set to 100% (n=3). The cytotoxicity of cells subjected to OGD

compared to the normoxia group showed no significant difference, as neither did the cytotoxicity of OGD+CysC treated cells compared to the cells treated with OGD only. (B) MTT cell viability assay. As in (A), measurements were done 24h after OGD treatment and CysC was added in both, normoxia and OGD conditions. The results are normalized to the normoxia group added with the solvent and set to 100% (n=3). The graph shows that the viability of cells treated with OGD has decreased but the difference was not significant compared to the normoxia group. The addition of CysC to cells treated with OGD did not change their viability either.

Snapses number are decreased 20 min after OGD treatment but rescued by treatment with either recombinant CysC or CysC loaded in EVs

To assess synaptic structures, we performed confocal microscopy of two known markers of dendrites and synapses, which is Microtubule Associated Protein 2 (MAP2) and synapsin1, respectively. MAP2 is a structural protein present at PSD that stabilizes the microtubules in the dendrites of differentiated neurons and is important for the cessation of cell division (Soltani et al., 2005). After 2 weeks in culture, MAP2 in hippocampal primary neurons is mainly compartmented to dendrites and absent or scarcely present in axons. The full extent of the postsynaptic dendritic tree can be appreciated by identifying MAP2 location in neuronal cell culture (Caceres et al., 1984). Synapsin1, a synaptic vesicle structural protein, is widely used as a presynaptic marker for synaptic quantification (García-Junco-Clemente et al., 2010, Gan and Südhof, 2019). We performed then immunocytochemistry (ICC) for MAP2 and synapsin1 followed by a 3D reconstruction of a whole neuron body as shown in Figure 9. To calculate the synaptic density, the number of synapsin1 positive puncta was referred to the dendritic area labeled with MAP2. The experiment was repeated 5 times, and in total more than 100 neurons per condition were analyzed (Norm+solvent (n=113), Norm+CysC (n=113), OGD+solvent (n=114), OGD+CysC (n=114)). Mean values of synaptic density per area and condition were then calculated and compared. As shown in Figure 9B, the synaptic density was significantly reduced after OGD ($p=0.0159$), whereas the addition of recombinant CysC after OGD ameliorated significantly the reduction of synaptic density ($p=0.0317$). Adding recombinant CysC did not alter the synaptic density of neurons in the normoxia groups.

Although how they deliver their content to recipient cells is not yet well-known (van

Niel et al., 2022), EVs are a good candidate for drug vehicles as they can cross the BBB (Saint-Pol et al., 2020). We thus tested if EVs loaded with recombinant CysC (cEVs) could also rescue synaptic structures as their not-encapsulated recombinant counterpart. We again established four groups: (a) normoxia with empty EVs (eEVs); (b) normoxia with cEVs; (c) OGD treatment followed by delivery of eEVs; (d) OGD treatment followed by delivery of cEVs. We chose 2 different concentrations for the treatment, 14 µl or 28 µl (corresponding to 4.8 x 10^9 particles/µl, 1.28 ng/µl of CysC), and 20 neurons were checked for each condition. As shown in figure 9 (D) and €, 20 min of OGD treatment decreased the synaptic density as shown before, but addition of 14 µl of cEVs (carrying around 18 ng of CysC) did not elicit significant protective effect compared to the eEVs group under OGD condition (ns, n=1). However, the addition of the double amount of cEVs leads to a significant protective effect on synapses compared to the eEVs group (p=0.0047, n=1). This last results are however very preliminary as there were only conducted once and to get a reliable conclusion, repetitions are planned for the near future.

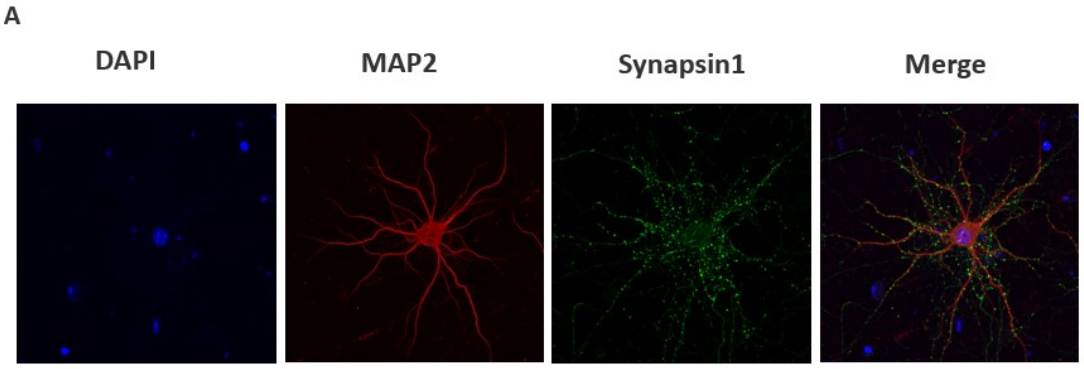

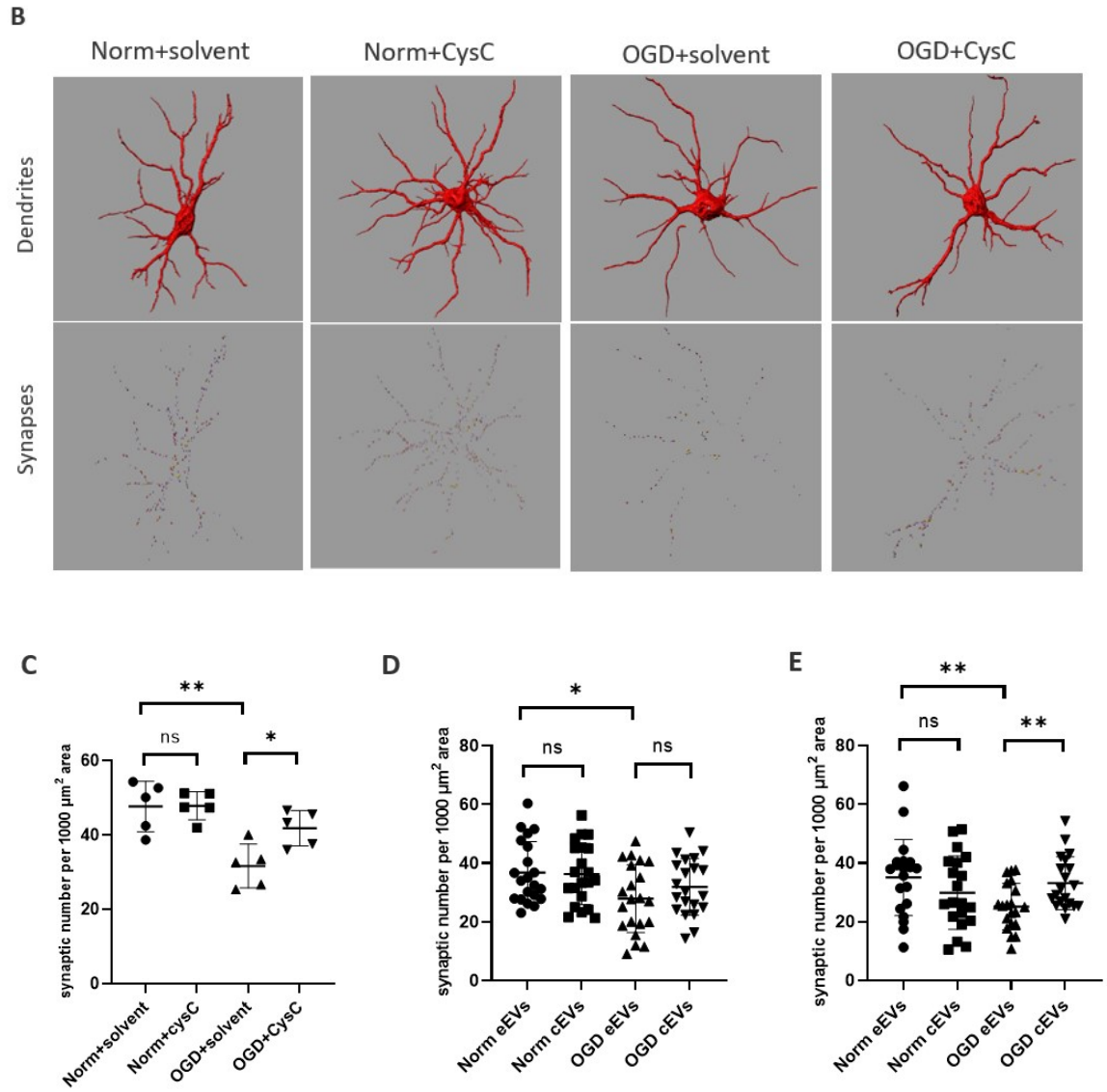

Fig.9. Recombinant CysC either in a free form or encapsulated in EVs added right after OGD treatment leads to the synaptic rescue. (A) Example of confocal images used for synaptic quantification of primary neuronal cell culture at DIV15. MAP2 is shown in red, synapsin1 in green, and DAPI, staining the nuclei, is in blue. (B). Example of a 3D reconstruction of the neuronal soma and dendrites (stained with MAP2) and synaptic puncta stained with synapsin1. (C) Bar graphs showing the quantifications of all the conditions examined. Under OGD treatment, the synaptic density was decreased compared to the normoxia (norm) group. The addition of recombinant CysC improves significantly synaptic survival (OGD+CysC), whereas CysC has no effect under normoxia conditions (Norm+CysC) (D) Addition of eEVs containing 18 ng CysC or eEVs does not show any positive effects in synaptic survival after OGD, however, (E) addition of EVs containing 36 ng CysC protected neuronal synaptic structures after OGD (ns. not significant, *p<0.05, **p<0.001).

In vivo experiments results

To assess whether the positive effects seen with CysC at the synaptic level *in vitro* were also present *in vivo*, we subjected male mice to tMCAO and deliver CysC loaded in EVs (or eEVs as a control) intraventricularly. We chose to start the treatment 6h after ischemia hypothesizing that this could be a feasible time-point for a treatment therapy in case of successful results. As we performed these experiments with our collaborators in the Nathan Kline Institute in New York (who loaded the EVs with CysC), we were blinded for cEVs and eEVs and we got two type of tubes, A and B. 6 wild-type mice for each condition were injected with EVs from group A and group B. One mouse injected with group B EVs was dead during the first night after stroke. Mice were assessed 24 h after injection.

No differences in stroke volume are observed in mice treated or not with CysC loaded in EVs 24h after injection.

The reaction of TTC (TTC to formazan) allows the visualization of the stroke area as the viable area turns red, whereas the affected area remains white. We quantified the ratio of the stroke area referred to the total brain area for each mouse with Image J software. As shown in Figure 10, infarct area ratios were not significantly different among the two mice groups.

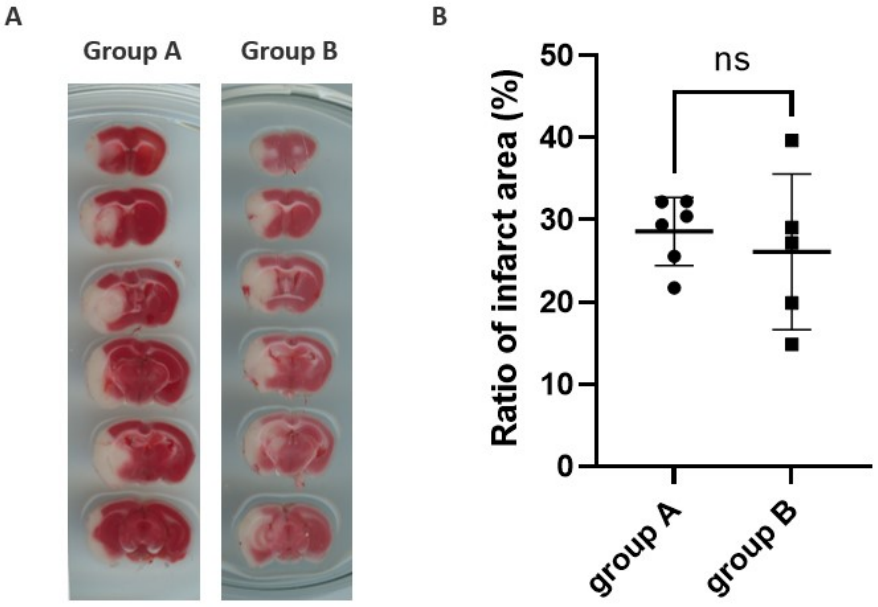

Fig.10. No differences in the stroke volume are observed between treatments with A or B EVs. (A) Example of a TTC-stained brain section 30 h after artery occlusion and 24 h after EV injection with either A or B EVs. (B) Bar graph showing the quantification of the stroke volume. No significant difference was observed between the ratio of infarct area in the two groups of treated mice (ns, not significant).

No differences in the amount of surviving neurons, and microglia or astrocyte activation in the stroke area after treatments with either non-loaded or CysC-loaded EVs

NeuN (neuron-specific nuclear protein) is a marker of the nucleus and cell body of most differentiated neuronal cell types (Purkinje cells, sympathetic ganglion cells, inner nuclear layer of retinal cells, inferior olivary and dentate neurons are not included) in rodents (Gusel'nikova and Korzhevskiy, 2015). After ischemic insult, its antigenicity attenuation or absence indicates neuronal injury (Ünal-Çevik et al., 2004), and we used it as an indicator of the stroke area in the brain cortex in our experiment. We also used isolectin B4 (a marker of vasculature and microglia in rodent brains) to assess microglia activation, and GFAP to detect astrocyte activation. As in some of the brains (mainly treated with B EVs), it seemed that more neurons were present in the stroke area, probably indicating higher survival, and therefore we quantified NeuN positive cells in the stroke area from three consecutive coronal slides (A (n=6), B (n=5)). However, as shown in the quantifications in 11C, no significant difference was observed between the two groups.

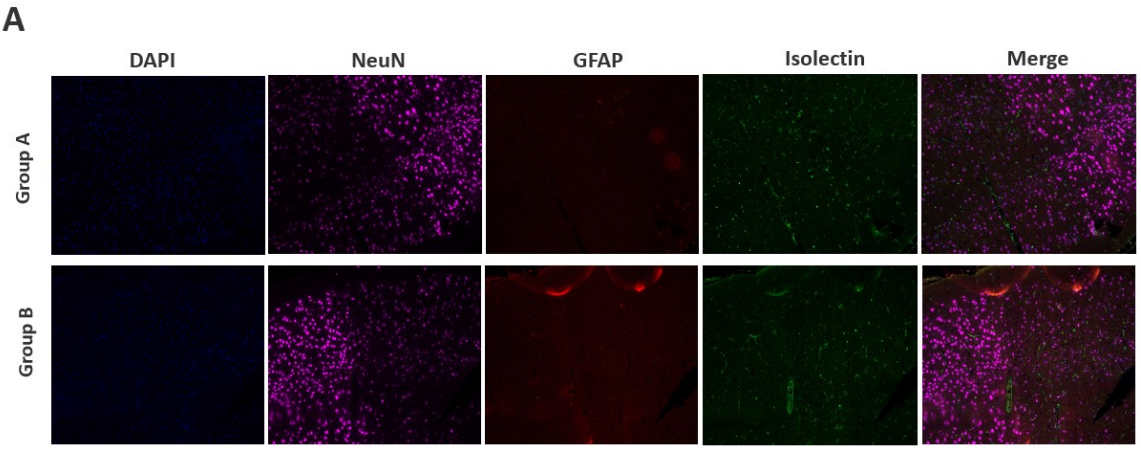

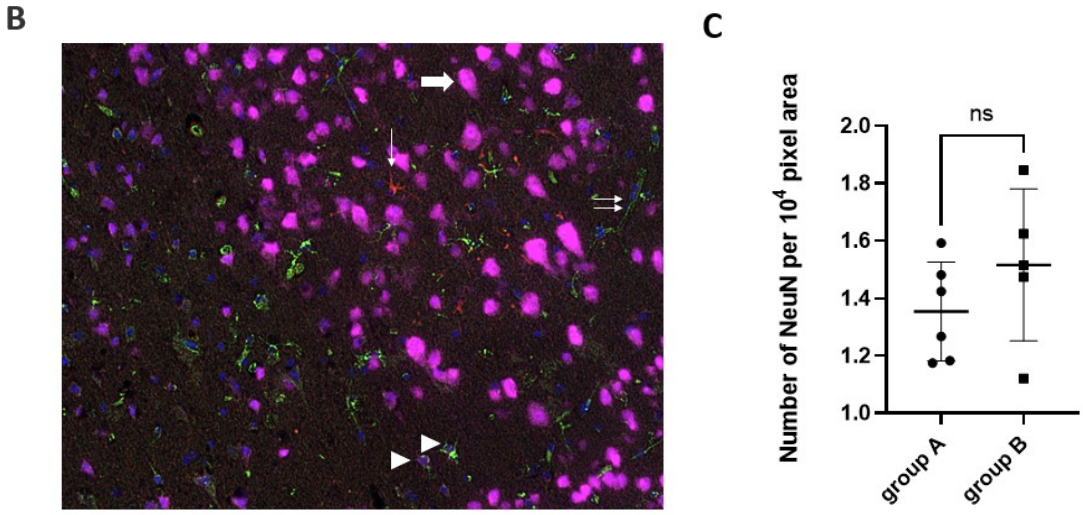

Fig.11. No differences in neuronal survival or microglia and astrocyte activation is observed between A and B treatment performed 6h after stroke and assessed 24 h after treatment. (A). Example of immunohistochemistry of the stroke area with NeuN (pink), isolectin B4 in green, GFAP in red, and DAPI (staining nuclei) in blue. The stroke area is characterized by reduced NeuN immunoreactivity. Microglia and astrocytes do not show a different pattern between two mice brain groups injected with EVs loaded with or without CysC respectively. (B). Magnified stroke and penumbra area from a brain corresponding to the A group. The thick single arrow indicates neuron body, single thin arrow indicates the reactive astrocyte, double thin arrows indicate a blood vessel, and arrowheads indicate microglia. (C) Bar graph showing the quantification of NeuN inside the stroke area comparing the two treatment groups, A and B. No significant difference is observed between them.

Of note, we also tried to quantify synaptic markers as in vitro, however, for the brain samples the background was so high that after trying with several markers we decided that we could not get any reliable results in this direction.

Discussion

Stroke and neuroplasticity

IS is characterized by high mortality and disability rate among patients. Though the pathophysiology of stroke has been intensively investigated for decades, due to the complexity and versatility of cellular signal transduction in the CNS under ischemic attack, and the limited time window of currently approved therapies, it is important to further explore novel neuroprotection and restoration therapies. Synapses are critical for neuronal signal transduction, and neuronal plasticity enhancement and synaptogenesis are the targets of rehabilitation treatment. In other words, rescuing synapses can ameliorate stroke damage and its associated neurological deficit.

In the acute phase of stroke, the brain tissue that is supplied by the occluded cerebral blood vessel is severely hypoperfused and rapidly evolves towards death, while the brain area that surrounds the infarct core, called the penumbra, is also hypoperfused but still viable (S. Liu et al., 2010). In the subacute phase, the salvageable tissue largely progresses to infarction (Kiran, 2012). In the chronic phase, the surviving neurons go through neuroanatomical remodeling, including axonal and dendritic growth (neuronal sprouting) followed by new synaptic connection establishment (synaptogenesis), which corresponds with behavioral recovery in rats (Stroemer et al., 1995). In a rat model of stroke and to understand the molecular pathways implicated in the sprouting mechanisms, a transcriptome study was done by comparing the transcriptome of neurons at the peri-infarct area presenting sprouting to neurons that were not presenting sprouting. The “sprouting transcriptome” unveiled a specific cellular program combining increased axonal guidance molecules, cytoskeletal remodeling proteins, cell-to-cell contact related-proteins, and proteins related to extracellular matrix interactions, fundamental for the sprouting in the penumbra (S. Li et al., 2010). As for synaptogenesis, activation of specific signaling pathways can decrease stroke volume and improve neurological function. For instance, the activation of the Caveolin-1/VEGF signaling pathway after exercise increases synaptic plasticity in the penumbra after I/R

as demonstrated in an animal stroke model (Xie et al., 2019). Astrocytes (which play multiphasic roles in modulating the progress of stroke) have a dual role in regulating synaptogenesis. On the one hand, it has been shown that the expression of thrombospondins 1 and 2, extracellular proteins mediating intercellular and cell-matrix interaction, were upregulated in astrocytes after stroke and that the inhibition of these two proteins was leading to neuronal sprouting, synaptogenesis, and behavioral recovery impairment (Liauw et al., 2008). On the other hand, it was demonstrated that a matricellular protein, SPARC (Secreted Protein, Acidic and Rich in Cysteine), was upregulated in astrocytes and microglia after hippocampal neuronal OGD and MCAO experiments. SPARC pre-treatment reduced OGD-induced neuronal death and loss of synapses, indicating also a beneficial role of astrocytes on synaptogenesis after stroke (Jones et al., 2018).

Proteomic changes after stroke

As synapses have their inherent ways to recover after stroke, in the present study we used synaptosomes to study how the proteome of synapses changes in a time-dependent manner after stroke, in the quest of finding proteins related to inner neuroprotection mechanisms that could be potentially used as therapeutic molecules. Synaptosomes were isolated from wild-type mice brains subjected to tMCAO or shams at 24h, 4d, and 7d after reperfusion. Proteomic analysis by mass spectrometry showed that at 24h after stroke, two protein clusters were upregulated, one constituted by ribosomal proteins (Ubiquitin A-52 Residue Ribosomal Protein Fusion Product 1, ribosomal protein L12, and 40S ribosomal protein S25 (encoded by Uba52, Rpl12, and Rps25 genes, respectively)) and the other by heat shock proteins (Heat shock-related 70 kDa protein, Heat shock 70 kDa protein 1A, and DnaJ homolog subfamily A member 1 (encoded by Hspa2, Hspa1a, and Dnaja1 genes, respectively)), indicating the enhancement of translational activity and activation of heat shock protein-mediated pro-survival mechanisms (J. Y. Kim et al., 2020). 4 and 7d after I/R, upregulated proteins in the stroke groups were related to protein metabolic processes with a cluster enriched in proteins from the lysosomal compartment (e.g., cathepsin B, cathepsin D, and CysC).

The lysosomes receive cargos for degradation from phagocytic, endocytic, and autophagic pathways (Figure 12) (C. Yang and Wang, 2021). They contain abundant hydrolases secreted from the ER, and are responsible for the maintenance of proteostasis in cells by degrading unwanted waste, modulating proteins, and recycling useful components for protein biosynthesis (Trivedi et al., 2020). Cathepsin B (encoded by Ctsb), a cysteine protease, and cathepsin D (encoded by Ctsd), an aspartic protease, are two potent lysosomal proteases and often used as the indicators of lysosomal proteolytic activity (X. Zhang et al., 2021, Hossain et al., 2021). CysC (encoded by Cst3), a cysteine protease inhibitor, is expressed and secreted by all the nucleated cells (Newman, 2002). The basic physiological functions of CysC include: regulation of the activity of intra- and extracellular cysteine proteases secreted or leaked from lysosomes of dying or diseased cells and antibacterial and antiviral functions (Mussap and Plebani, 2004). After an ischemic attack, the lysosomal membrane permeabilization is induced by ROS accumulation, leading to subsequent proteolytic damage and lysosomal apoptosis (Hafner Česen et al., 2012). The upregulation of cathepsin B and D is a strong indicator of the enhancement of lysosomal activity at 4-7d after stroke, and the upregulation of CysC is probably an attempt to ameliorate the proteolytic damage caused by leaked cathepsins from permeabilized lysosomes in stroke.

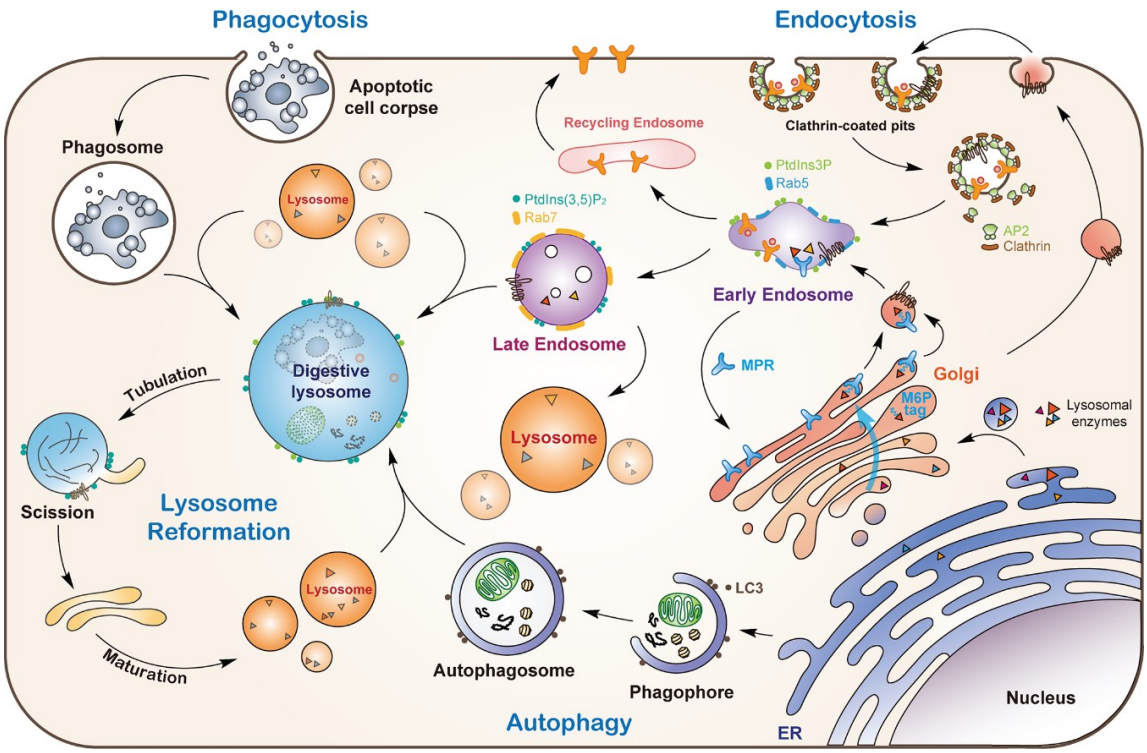

Fig.12. Biogenesis and multiple cargo sources of lysosomes. As for the biogenesis: Lysosomal hydrolases are produced in the ER-Golgi compartments, and then delivered through binding with MPR (mannose 6-P receptor) to reach the early endosomes. The lysosomal membrane proteins are also produced at the ER-Golgi system, some are delivered to the early endosomes in an MPR-dependent manner (direct pathway), and some are first sent to the plasma membrane to be later integrated into the early endosomal membrane (indirect pathway). The early endosomes (enriched in Rab5) progressively mature into late endosomes (enriched in Rab7) and eventually mature into lysosomes. As for the cargo sources, this can be originated by: (i) phagocytosis: phagosomes containing phagocytosed cargos, mature and then fuse with lysosomes. (ii) endocytosis: the fusion of late endosomes with lysosomes. (iii): autophagy: phagophores produced from the ER engulfs unwanted proteins and organelles, and further mature into autophagosomes to fuse with lysosomes. Lysosomes can be regenerated through tubulation and scission from the digestive lysosomes to form protolysosomes, which further mature into functional lysosomes. (C. Yang and Wang, 2021)

It has been shown that proteome changes in the ischemic brain (full tissue) at the very early phase (1h after I/R) were also mainly associated with ribosomal activity upregulation (Agarwal et al., 2020). At around 3 days after stroke, the upregulated proteins were mainly involved in the acute cellular responses such as blood coagulation and complement-mediated immune response (Gu et al., 2021). At the subacute to the chronic phase of stroke (7d-28d), both innate and adaptive immune responses were upregulated, lysosomal structures and functions were restored, and neuronal cytoskeletal and synaptic remodeling pathways were active (Gu et al., 2021, Wen et al.,

2019). The results of our proteomic analysis from synaptosomes are partially similar to the previous studies. The trace of immune response is less obvious probably because our proteomic analysis was restricted to synapses and not the whole brain tissue. Our results suggest that, in the acute phase of stroke, synapses go through significant changes in biological processes and morphology in response to ischemic attack. In the subacute phase, the lysosomal proteolytic activity gradually become dominant, indicating a high rate of protein turnover, probably implicating that repairing processes are being set up.

At 24h, CysC was identified in two stroke animals but not in the sham group, however, CysC was detected in western blot in all the animals and significantly upregulated at this time point. As for an explanation, it could be that the mass spectrometry was not as sensitive as the western blot. At 4d after stroke, CysC was found upregulated in the stroke group in both MS analysis and western blot, whereas, at 7d after stroke, CysC levels were detectable in all animals but the levels of expression were not significantly different in the two groups. This temporal dynamic change of CysC indicates a potential role of CysC in the acute phase of stroke.

The role of CysC in IS

CysC is postulated to have protective effects in stroke as it has been shown that their pharmacological use as an inhibitor of cathepsins (such as cathepsin B and cathepsin L, upregulated after IS could rescue hippocampal neurons from ischemic damage (Yamashima et al., 1998). CysC overexpression increased the expression level of caveolin-1 and occludin thus enhancing the BBB integrity after ischemia insult in a mouse stroke model (Yang et al., 2020b). Exogenous CysC added to primary neuronal culture protects neurons from various toxic stimuli, such as nutrient deprivation or oxidative stress through autophagy induction (Tizon, Sahoo, et al., 2010). Moreover, CysC-loaded EVs were shown to increase neuronal viability under nutrition deprivation in neuronal cell cultures (Pérez-González et al., 2019). Interestingly, a recent study showed that CysC is not only important for the neuroprotection effect against ischemic insult after hyperbaric oxygen pretreatment, but the intracerebroventricular injection of

CysC after MCAO alone reduced cerebral ischemic injury (Fang et al., 2017). Further investigations demonstrated that the neuroprotection of CysC was related to the enhancement of autophagy flux and the preservation of the lysosomal membrane integrity (Fang et al., 2019). (Figure 13) From our study, we propose that another mechanism whereby CysC could exert neuroprotection is found at the synaptic level.

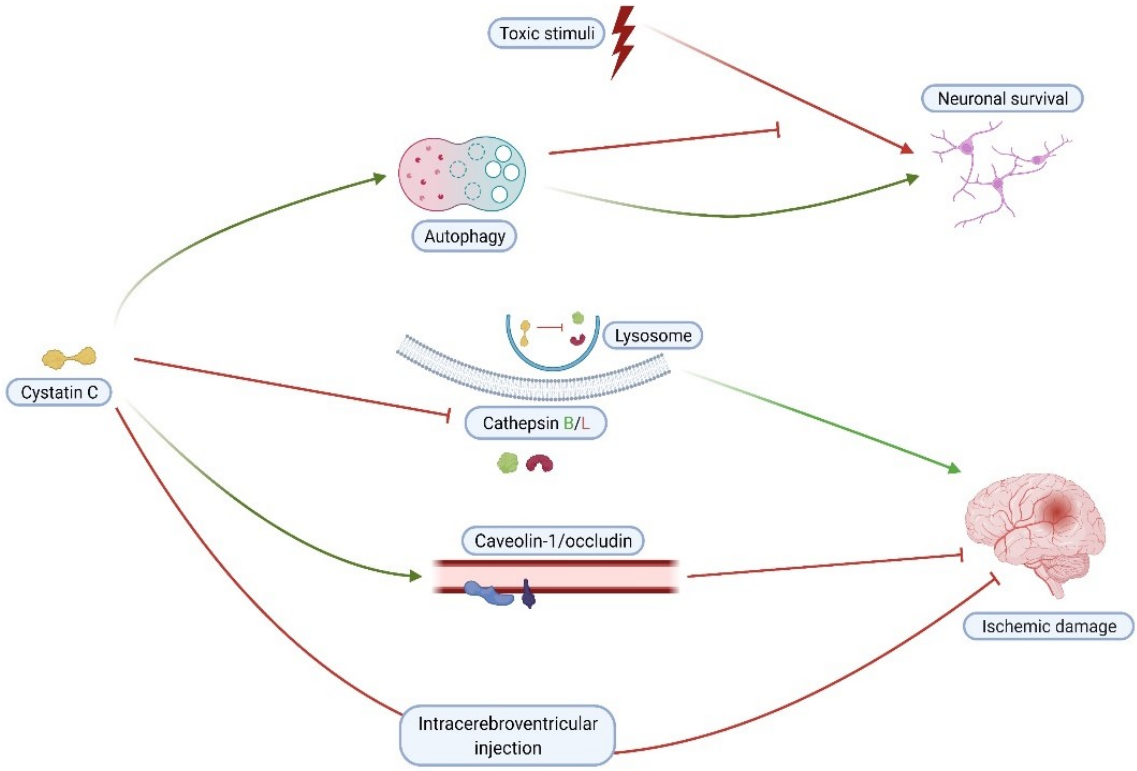

Fig.13. Illustration of the role of CysC in neuronal survival under toxic stimuli and stroke pathology. Previous *in vitro* studies demonstrated that CysC could protect neuronal cells against toxic stimuli, such as oxidative stress and nutrient deprivation, through activation of the autophagic pathway. *In vivo* studies showed that CysC could be an important therapy in stroke through BBB barrier integrity maintenance, and inhibition of the activity of leaked lysosomal cathepsins. A previous study injecting CysC intracerebroventricularly showed decreased stroke volume in rats compared to the control group (Tizon, Sahoo, et al., 2010, Pérez-González et al., 2019a, Yang et al., 2020b, Fang et al., 2019).

Recombinant CysC could protect neuronal synapses after OGD treatment

Among the differentially expressed proteins between the stroke and sham groups, CysC was found significantly upregulated in the synaptosomes of the stroke group at 24h and 4d after stroke while at 7d after stroke, CysC is not significantly upregulated anymore.

Thus, we hypothesized that it might also exert its protective effect through maintaining the synaptic structure or promoting synaptogenesis, an effect that has never been investigated before. To set up our study, we first tested neuron cell viability in neuron cell culture, to mimic the penumbra conditions, i.e, where neurons are still viable but are electrically silent (probably due to the loss of synaptic contacts). OGD is a widely used *in vitro* experimental model to mimic clinical stroke, and the post reoxygenation is to mimic reperfusion after clinical stroke. Depending on the protocols, cellular exposure to OGD varies between 20 min to hours (Z. Zhang et al., 2020, Rayasam et al., 2022, Y. Li et al., 2022). After trying different time points, we chose a treatment of 20 min of OGD as we could demonstrate that neurons were as viable as the non-treated, but under this OGD conditions, they significantly lost synapsis. This is in agreement with the knowledge that synaptic ultrastructural and functional changes happen before neuronal death (Hinman et al., 2013). We then treated the neuronal cultures with exogenous recombinant CysC right after the ODG as it was demonstrated that exogenous CysC could be internalized by many cancer cell lines in cell culture starting from 5 min after incubation (Ekström et al., 2008) and that the cysteine protease inhibitory ability of CysC was conserved after internalization (Sheikh et al., 2021). The addition of 2 µg of recombinant CysC significantly increased the synaptic density, indicating that either CysC protects the synaptic structure under OGD or that CysC is involved in synaptogenesis. A recent study has found that the constant active autophagic activity after I/R increased the workload of autolysosomal protein degradation and caused the dysfunction of lysosomes, manifested with volume enlargement and decrease of proteases activity (cathepsin B and D), leading to synaptic abnormalities such as decreased RRP size and PSD thickness, and increased synaptic space width. Further proteomic analysis indicated this synaptic impairment may be caused by the disrupted turnover of synaptic proteins (X. Zhang et al., 2021). And CysC was found involved in the maintenance of lysosome membrane integrity and in the increase of autophagosome formation in stroked animals (Fang et al., 2019). Thus we hypothesize that CysC may help to preserve synaptic structures after ischemia through stabilization of the neuronal

lysosomal membrane and enhancement of autophagy-lysosomal activity. Although autophagic activity was historically considered to be harmful, as its inhibition reduced stroke volume in neonatal rats (Puyal and Clarke, 2009). Recent studies suggest that restoration or maintenance of autophagy-lysosomal normal activity after stroke is neuroprotective (Y. Liu et al., 2019, Hossain et al., 2021, Y. Zhang et al., 2022). It could be that the autophagosomes gather abnormal and obsolete proteins to be degraded in autolysosomes, which is beneficial, as it tries to maintain protein homeostasis at the cytoplasm and synapses; but on the other hand, excessive autophagy might exhaust the lysosomal proteolytic capability, leading to autophagic cell death. The inhibition of lysosomal membrane permeability by CysC under ischemic attack is thus helpful to sustain normal lysosomal function and the protein homeostasis at the synapses, promoting the maintenance of synaptic structures.

CysC-loaded EVs may be used as delivery tools as they also protect neuronal synapses after OGD

EVs can be internalized by recipient cells although the exact mechanism is still not yet fully elucidated, especially how the content of EVs can be delivered to the cytosol of recipient cells (Kwok et al., 2021). Among the described uptake mechanisms, receptor-mediated endocytosis, phagocytosis, micropinocytosis, and membrane fusion have been described (Mulcahy et al., 2014). Endocytosis seems to be the dominant entry method, however, it is worth noting that the uptake could include more than one exclusive mechanism of internalization and it is probably cell type-dependent (Mulcahy et al., 2014). Over decades, the drug vehicle system has been developed to improve the therapeutic effect through refining drug pharmacokinetics and pharmacodynamics, but drug vectors, such as liposomes, could not deliver drugs in an efficiently targeted way, due to the clearance by the innate immune system, severe hypersensitive reaction, and the accumulation in the spleen (Sercombe et al., 2015). EVs are proposed as natural bioactive drug vehicles, which is very interesting for the therapeutic delivery into the brain as they have the ability to cross the BBB (Sercombe et al., 2015). Moreover, they are more propense to be better internalized than synthetic vectors, have lower toxicity to

recipient cells, and that do not trigger an immune response (Elsharkasy et al., 2020). CysC loaded on EVs protected primary neuronal cells and primary cortical smooth muscle cells from nutrient deprivation (Pérez-González et al., 2019). In collaboration with the group that published these results (the group of professor Levy from the Department of Biochemistry and Molecular Pharmacology, NYU Langone Health, New York) and as we observed the protective effect of recombinant CysC on synapses under OGD, we also tested if cEVs could show the same protective effect, as a proof-of-concept of EVs as therapeutic tools in this setting. EVs were loaded with two different doses of CysC. The low dose of CysC in EVs was not showing any protective effect when delivered to the neurons after OGD, however, preliminary experiments with the higher dose showed similar protection obtained when free recombinant CysC was administrated. Thus the protective effect of CysC through the delivery of EVs is a dose-dependent effect, which is in line with the dose-dependent protective property of CysC on primary neuronal cells under B27 supplement deprivation (Tizon et al., 2010). However, the experiment with high CysC was only conducted once and remains to be verified through the repetition of more experiments.

Modulation effect of CysC-loaded EVs in stroked brains

There are several ways that CysC can be protective after ischemia *in vivo*. Kato et al showed that exogenous CysC was the factor that induced the differentiation of embryonic cells (ES) to neural stem cells (NSC) with a high capability of differentiation to neurons, astrocytes, and oligodendrocytes *in vitro* and *in vivo* (Kato et al., 2006). Apart from this, as previously mentioned, CysC is also associated with BBB preservation, cysteine protease inhibition, autophagy enhancement, and lysosomal system stabilization after stroke. Because cEVs protected the synapses *in vitro* after OGD and to further explore a possible protective effect of CysC loaded in EVs *in vivo*, we designed an experiment to deliver cEVs to a mouse model of stroke (tMCAO). We decided to inject cEVs 6h after stroke as this would be a plausible time-window treatment. In our experiments, the stroke volume between the CysC-treated group and vehicle-treated group did not show significant differences, nor did the astrocyte and

microglia activation degree, nor the amount of surviving neurons in the core of the stroke.

In fact, as mentioned before, it has already been shown that intracerebroventricular injection of CysC could improve stroke outcomes compared to the control group (Fang et al., 2017). The discrepancy with our results might be due to the different experiment design, as we administrated CysC 6 h after artery occlusion (thinking as a possible clinical treatment) instead of 30 min after reperfusion. Moreover, the vehicle used to deliver CysC in the previous study was artificial cerebral spinal fluid, and in our case EVs, which could have an influence on the uptake. Moreover, the amount of CysC loaded to show the effect might also matter, thus probably a higher amount of cEVs (or CysC loaded in these EVs) is required for an appreciable change in stroke volume and neuronal rescue.

Conclusion

Taken together, CysC was upregulated at 24h and 4d but not at 7d after stroke in the synaptosomes of penumbra. Recombinant CysC and cEVs added in the primary neuronal culture have promoted the neuronal synaptic density 24h after OGD treatment compared to the control groups. However, cEVs didn’t elicit obvious protective effect against stroke *in vivo*. It is indicated that CysC can assist the maintenance of synaptic structure under ischemic attack and could be a new therapy for stroke, but the underlying mechanism remains elusive. The translation to bedside requires further optimization of the treatment scheme.

Summary

Ischemic stroke is still a global challenge due to the limited treatment time window and the high rate of disability and mortality. Synaptic recovery is the prerequisite for neuronal functional restoration. We hypothesize that investigation of the inherent mechanism involved in synaptic remodeling could provide a new perspective for stroke treatment. Therefore, in this study, we have performed a temporal proteomic analysis of synaptosomes (i.e., synaptic terminals purified from brain) after stroke. Cystatin C (CysC), a cystatin protease known to inhibit cathepsins, and shown to be protective when exogenously administered after ischemic damage, was found significantly upregulated at 24h and 4d, but not at 7d after stroke. These results were validated by western blot analysis. To understand a possible mechanism whereby CysC could contribute to the synaptic rescue, we challenged neuronal cultures with an in vitro model of stroke and treated them with or without recombinant CysC (in a free form or inside extracellular vesicles (cEVs)). We found that free CysC and cEVs protected the synaptic structures after ischemic damage. We then performed *in vivo* analysis by inoculating cEVs to stroke mice. We could not observe significant changes related ge to stroke volume, astrocyte and microglia activation, and neuronal viability, possibly due to the time-point chosen to observe the effects (24h). This study demonstrates that CysC administration might be a promising therapy against stroke but further investigation is needed for an effective therapeutic plan.

Zusammenfassung

Der ischämische Schlaganfall stellt aufgrund des begrenzten Behandlungszeitfensters und der hohen Behinderungs- und Sterblichkeitsrate noch immer eine globale Herausforderung dar. Die Erholung der Synapsen ist die Voraussetzung für die Wiederherstellung der neuronalen Funktionen und das Überleben von Nervenzellen. Wir sind überzeugt, dass die Untersuchung der Mechanismen, die an der synaptischen Remodellierung beteiligt sind, eine neue Perspektive für die Schlaganfallbehandlung eröffnen könnte. Daher haben wir in dieser Studie eine zeitliche Proteomanalyse von

Synaptosomen (das sind aus Hirngewebe isolierte synaptische Endigungen) nach dem Schlaganfall durchgeführt. Cystatin C (CysC), eine Cystatin-Protease, die bekanntermaßen Cathepsine hemmt und sich bei exogener Verabreichung nach ischämischer Schädigung als schützend erwiesen hat, war 24 Stunden und 4 Tage, nicht aber 7 Tage nach dem Schlaganfall signifikant hochreguliert. Diese Ergebnisse wurden durch eine Westernblot-Analyse bestätigt. Um einen möglichen Mechanismus zu verstehen, durch den CysC zur Rettung von Synapsen beitragen könnte, haben wir neuronale Kulturen mit einem In-vitro- Schlaganfallmodell behandelt und sie mit oder ohne rekombinantes CysC (in freier Form oder verpackt in extrazellulären Vesikeln (cEVs)) behandelt. Wir fanden heraus, dass freies CysC und cEVs die synaptischen Strukturen nach einer ischämischen Schädigung schützen. Anschließend führten wir eine In-vivo-Analyse durch, indem wir Mäusen nach Schlaganfall intrazerebral cEVs verabreichten. Wir konnten keine signifikanten Veränderungen in Bezug auf das Schlaganfallvolumen, die Astrozyten- und Mikrogliaaktivierung und die neuronale Lebensfähigkeit beobachten, was möglicherweise auf den für die Beobachtung der Auswirkungen gewählten Zeitpunkt (24 Stunden nach Schlaganfall) zurückzuführen ist. Zusammenfassend lässt sich sagen, dass die Verabreichung von CysC eine vielversprechende Therapie gegen Schlaganfall sein könnte, aber für einen wirksamen Therapieplan sind weitere Untersuchungen erforderlich.

References

Agarwal A, Park S, Ha S, Kwon JS, Khan MR, Kang BG, Dawson TM, Dawson VL, Andrabi SA, Kang SU (2020) Quantitative mass spectrometric analysis of the mouse cerebral cortex after ischemic stroke. PLoS One. 15(4):e0231978.

Alawieh A, Farris Langley E, Feng W, Spiotta A, Tomlinson S (2020) Complement-Dependent Synaptic Uptake and Cognitive Decline after Stroke and Reperfusion Therapy. J Neurosci. 40(20): 4042-4058.

Astrup J, Symon L, Branston NM, Lassen NA (1977) Cortical evoked potential and extracellular K+ and H+ at critical levels of brain ischemia. Stroke. 8(1):51–57.

Ayata C, Lauritzen M (2015) Spreading Depression, Spreading Depolarizations, and the Cerebral Vasculature. Physiol Rev. 95(3):953-993.

Back T (1998) Pathophysiology of the Ischemic Penumbra—Revision of a Concept. Cell Mol Neurobiol. 18(6):621–638.

Bai F, Witzmann FA (2007) Synaptosome proteomics. Subcell Biochem. 43:77–98.

Balbinot G, Schuch CP (2019) Compensatory relearning following stroke: Cellular and plasticity mechanisms in rodents. Front Neurosci. 12:1023.

Ballarin B, Tymianski M (2018) Discovery and development of NA-1 for the treatment of acute ischemic stroke. Acta Pharmacol Sin. 39(5):661-668..

Bandera E, Botteri M, Minelli C, Sutton A, Abrams KR, Latronico N (2006) Cerebral blood flow threshold of ischemic penumbra and infarct core in acute ischemic stroke: A systematic review. Stroke. 37(5):1334–1339.

Batool S, Raza H, Zaidi J, Riaz S, Hasan S, Syed NI (2019) Synapse formation: from cellular and molecular mechanisms to neurodevelopmental and neurodegenerative disorders. J Neurophysiol. 121(4):1381–1397.

Benveniste M, Mayer ML (1991) Kinetic analysis of antagonist action at N-methyl-D-aspartic acid receptors. Two binding sites each for glutamate and glycine. Biophys J. 59(3):560–573.

Boeckers TM (2006) The postsynaptic density. Cell Tissue Res. 326(2):409–422.

Bolay H, Gürsoy-Özdemir Y, Sara Y, Onur R, Can A, Dalkara T (2002) Persistent defect in transmitter release and synapsin phosphorylation in cerebral cortex after transient moderate ischemic injury. Stroke. 33(5):1369–1375.

Boode B, Welzen V, Franke C, Van Oostenbrugge R (2007) Estimating the number of stroke patients eligible for thrombolytic treatment if delay could be avoided. Cerebrovasc Dis. 23(4):294–298.

Borges-Merjane C, Kim O, Correspondence PJ, Jonas P (2020) Functional Electron Microscopy, "'Flash and Freeze,'" of Identified Cortical Synapses in Acute Brain Slices NeuroResource Functional Electron Microscopy, " 'Flash and Freeze,'" of Identified Cortical Synapses in Acute Brain Slices. Neuron. 105:992–1006.

Brenna S, Altmeppen HC, Mohammadi B, Rissiek B, Schlink F, Ludewig P, Krisp C, Schlüter H, Failla AV, Schneider C, Glatzel M, Puig B, Magnus T (2020) Characterization of brain-derived extracellular vesicles reveals changes in cellular origin after stroke and enrichment of the prion protein with a potential role in

cellular uptake. J Extracell Vesicles. 9(1):1809065.
Brown CE, Wong C, Murphy TH (2008) Rapid Morphologic Plasticity of Peri-Infarct Dendritic Spines After Focal Ischemic Stroke. Stroke. 39(4):1286–1291.
Caceres A, Banker G, Steward O, Binder L, Payne M (1984) MAP2 is localized to the dendrites of hippocampal neurons which develop in culture. Dev Brain Res. 13(2):314–318.
Ceulemans AG, Zgavc T, Kooijman R, Hachimi-Idrissi S, Sarre S, Michotte Y (2010) The dual role of the neuroinflammatory response after ischemic stroke: Modulatory effects of hypothermia. J Neuroinflammation. 7(1):1–18.
Chamorro Á, Dirnagl U, Urra X, Planas AM (2016) Neuroprotection in acute stroke: Targeting excitotoxicity, oxidative and nitrosative stress, and inflammation. Lancet Neurol. 15(8):869–881.
Chen M, Lu TJ, Chen XJ, Zhou Y, Chen Q, Feng XY, Xu L, Duan WH, Xiong ZQ (2008) Differential roles of NMDA receptor subtypes in ischemic neuronal cell death and ischemic tolerance. Stroke. 39(11):3042–3048.
Cheng ZJ, Dai TM, Shen YY, He J Le, Li J, Tu JL (2018) Atorvastatin Pretreatment Attenuates Ischemic Brain Edema by Suppressing Aquaporin 4. J Stroke Cerebrovasc Dis. 27(11):3247–3255.
Cisani F, Olivero G, Usai C, Van Camp G, Maccari S, Morley-Fletcher S, Pittaluga AM (2021) Antibodies Against the NH 2-Terminus of the GluA Subunits Affect the AMPA-Evoked Releasing Activity: The Role of Complement. Front Immunol. 12:586521.
Cotman CW, Taylor D (1972) ISOLATION AND STRUCTURAL STUDIES ON SYNAPTIC COMPLEXES FROM RAT BRAIN. J Cell Biol. 55(3):696–711.
D'Ambrosio AL, Pinsky DJ, Connolly ES (2001) The Role of the Complement Cascade in Ischemia/Reperfusion Injury: Implications for Neuroprotection. Mol Med 2001 76. 7(6):367–382.
del Zoppo GJ (2010) Acute anti-inflammatory approaches to ischemic stroke. Ann N Y Acad Sci. 1207(1):143–148.
Doyle LM, Wang MZ (2019) Overview of Extracellular Vesicles, Their Origin, Composition, Purpose, and Methods for Exosome Isolation and Analysis. Cells. 8(7):727.
Dreier JP (2011) The role of spreading depression, spreading depolarization and spreading ischemia in neurological disease. Nat Med. 17(4):439–447.
Easton AS (2013) Neutrophils and stroke - Can neutrophils mitigate disease in the central nervous system? Int Immunopharmacol.17(4):1218-25.
Ekström U, Wallin H, Lorenzo J, Holmqvist B, Abrahamson M, Avilés FX (2008) Internalization of cystatin C in human cell lines. FEBS J. 275(18):4571–4582.
Elsharkasy OM, Nordin JZ, Hagey DW, de Jong OG, Schiffelers RM, Andaloussi S EL, Vader P (2020) Extracellular vesicles as drug delivery systems: Why and how? Adv Drug Deliv Rev. 159:332–343.
Evans GJO (2015) The Synaptosome as a Model System for Studying Synaptic Physiology. Cold Spring Harb Protoc. 2015(5):421-424.

Fang Z, Deng J, Wu Z, Dong B, Wang S, Chen X, Nie H, Dong H, Xiong L (2017) Cystatin C is a Crucial Endogenous Protective Determinant Against Stroke. Stroke. 48(2):436–444.

Fang Z, Feng Y, Li Y, Deng J, Nie H, Yang Q, Wang S, Dong H, Xiong L (2019) Neuroprotective Autophagic Flux Induced by Hyperbaric Oxygen Preconditioning is Mediated by Cystatin C. Neurosci Bull. 35(2):336–346.

Feigin VL, Stark BA, Johnson CO, Roth GA, Bisignano C, Abady GG, Abbasifard M, Abbasi-Kangevari M, Abd-Allah F, Abedi V, Abualhasan A, Abu-Rmeileh NME, Abushouk AI, Adebayo OM, Agarwal G, Agasthi P, Ahinkorah BO, Ahmad S, Ahmadi S, … Murray CJL (2021) Global, regional, and national burden of stroke and its risk factors, 1990-2019: A systematic analysis for the Global Burden of Disease Study 2019. Lancet Neurol. 20(10):1–26.

Fisher M, Bastan B (2012) Identifying and utilizing the ischemic penumbra. Neurology. 79(13 Suppl 1):S79-85.

Gan KJ, Südhof TC (2019) Specific factors in blood from young but not old mice directly promote synapse formation and NMDA-receptor recruitment. Proc Natl Acad Sci U S A. 116(25):12524–12533.

García-Junco-Clemente P, Cantero G, Gómez-Sánchez L, Linares-Clemente P, Martínez-López JA, Luján R, Fernández-Chacón R (2010) Cysteine string protein-α prevents activity-dependent degeneration in GABAergic synapses. J Neurosci. 30(21):7377–7391.

Gauberti M, De Lizarrondo SM, Vivien D (2016) The “inflammatory penumbra” in ischemic stroke: From clinical data to experimental evidence. Eur Stroke J. 1(1):20–27.

Gauberti M, Montagne A, Marcos-Contreras OA, Le Béhot A, Maubert E, Vivien D (2013) Ultra-sensitive molecular MRI of vascular cell adhesion molecule-1 reveals a dynamic inflammatory penumbra after strokes. Stroke. 44(7):1988–1996.

Gauthier S, Kaur G, Mi W, Tizon B, Levy E (2011) Protective mechanisms by cystatin C in neurodegenerative diseases. Front Biosci - Sch. 3 S(2):541–554.

Gelderblom M, Leypoldt F, Steinbach K, Behrens D, Choe CU, Siler DA, Arumugam T V., Orthey E, Gerloff C, Tolosa E, Magnus T (2009) Temporal and spatial dynamics of cerebral immune cell accumulation in stroke. Stroke. 40(5):1849–1857.

George PM, Steinberg GK (2015) Novel Stroke Therapeutics: Unraveling Stroke Pathophysiology and Its Impact on Clinical Treatments. Neuron. 2015 Jul 15;87(2):297-309.

Gold L, Lauritzen M (2002) Neuronal deactivation explains decreased cerebellar blood flow in response to focal cerebral ischemia or suppressed neocortical function. Proc Natl Acad Sci U S A. 99(11):7699–7704.

Golding EM, Steenberg ML, Johnson TD, Bryan RM (2001) Nitric oxide in the potassium-induced response of the rat middle cerebral artery: A possible permissive role. Brain Res. 889(1–2):98–104.

Gu RF, Fang T, Nelson A, Gyoneva S, Gao B, Hedde J, Henry K, Peterson E, Burkly

LC, Wei R (2021) Proteomic Characterization of the Dynamics of Ischemic Stroke in Mice. J Proteome Res. 20(7):3689–3700.

Gusel'nikova V V., Korzhevskiy DE (2015) NeuN As a Neuronal Nuclear Antigen and Neuron Differentiation Marker. Acta Naturae. 7(2):42-47.

Hacioglu C, Kar F, Kanbak G (2021) Ex Vivo Investigation of Bexarotene and Nicotinamide Function as a Protectıve Agent on Rat Synaptosomes Treated with Aβ(1-42). Neurochem Res. 46(4):804–818.

Hafner Česen M, Pegan K, Špes A, Turk B (2012) Lysosomal pathways to cell death and their therapeutic applications. Exp Cell Res. 318(11):1245–1251.

Haney MJ, Klyachko NL, Zhao Y, Gupta R, Plotnikova EG, He Z, Patel T, Piroyan A, Sokolsky M, Kabanov A V., Batrakova E V. (2015) Exosomes as Drug Delivery Vehicles for Parkinson's Disease Therapy. J Control Release. 207:18-30.

Heiss W -D, Rosner G (1983) Functional recovery of cortical neurons as related to degree and duration of ischemia. Ann Neurol. 14(3):294–301.

Heiss WD (2016) Malignant MCA infarction: Pathophysiology and imaging for early diagnosis and management decisions. Cerebrovasc Dis. 41(1–2):1–7.

Hergeth SP, Schneider R (2015) The H1 linker histones: multifunctional proteins beyond the nucleosomal core particle. EMBO Rep. 16(11):1439-1453.

Hinman JD, Rasband MN, Carmichael ST (2013) Remodeling of the axon initial segment after focal cortical and white matter stroke. Stroke. 44(1):182-189.

Hirokawa N, Sobue K, Kanda K, Harada A, Yorifuji H (1989) The cytoskeletal architecture of the presynaptic terminal and molecular structure of synapsin 1. J Cell Biol. 108(1):111–126.

Hofmeijer J, Van Putten MJAM (2012) Ischemic cerebral damage: An appraisal of synaptic failure. Stroke. 43(2):607–615.

Hossain MI, Marcus JM, Lee JH, Garcia PL, Singh VK, Shacka JJ, Zhang J, Gropen TI, Falany CN, Andrabi SA (2021) Restoration of CTSD (cathepsin D) and lysosomal function in stroke is neuroprotective. Autophagy. 17(6):1330–1348.

Ito U, Kuroiwa T, Nagasao J, Kawakami E, Oyanagi K (2006) Temporal profiles of axon terminals, synapses and spines in the ischemic penumbra of the cerebral cortex: Ultrastructure of neuronal remodeling. Stroke. 37(8):2134–2139.

Jayaraj RL, Azimullah S, Beiram R, Jalal FY, Rosenberg GA (2019) Neuroinflammation: Friend and foe for ischemic stroke. J Neuroinflammation. 16(1):142.

Jiang CT, Wu WF, Deng YH, Ge JW (2020) Modulators of microglia activation and polarization in ischemic stroke (Review). Mol Med Rep. 21(5):2006-2018.

Jin R, Yang G, Li G (2010) Inflammatory mechanisms in ischemic stroke: role of inflammatory cells. J Leukoc Biol. 87(5):779–789.

Johnstone RM, Adam M, Hammond JR, Orr L, Turbide C (1987) Vesicle formation during reticulocyte maturation. Association of plasma membrane activities with released vesicles (exosomes). J Biol Chem. 262(19):9412–9420.

Jones E V., Bernardinelli Y, Zarruk JG, Chierzi S, Murai KK (2018) SPARC and GluA1-containing AMPA receptors promote neuronal health following CNS injury. Front Cell Neurosci. 12:22.

Kalia M, Meijer HGE, van Gils SA, van Putten MJAM, Rose CR (2021) Ion dynamics at the energy-deprived tripartite synapse. PLoS Comput Biol. 17(6):e1009019..

Kang L, Yu H, Yang X, Zhu Y, Bai X, Wang R, Cao Y, Xu H, Luo H, Lu L, Shi MJ, Tian Y, Fan W, Zhao BQ (2020) Neutrophil extracellular traps released by neutrophils impair revascularization and vascular remodeling after stroke. Nat Commun. 11(1):2488.

Kato T, Heike T, Okawa K, Haruyama M, Shiraishi K, Yoshimoto M, Nagato M, Shibata M, Kumada T, Yamanaka Y, Hattori H, Nakahata T (2006) A neurosphere-derived factor, cystatin C, supports differentiation of ES cells into neural stem cells. Proc Natl Acad Sci U S A. 103(15):6019–6024.

Kaufman AM, Milnerwood AJ, Sepers MD, Coquinco A, She K, Wang L, Lee H, Craig AM, Cynader M, Raymond LA (2012) Opposing roles of synaptic and extrasynaptic NMDA receptor signaling in cocultured striatal and cortical neurons. J Neurosci. 32(12):3992–4003.

Kim JY, Kim JW, Yenari MA (2020) Heat shock protein signaling in brain ischemia and injury. Neurosci Lett. 715:134642..

Kim SW, Lee H, Lee HK, Kim ID, Lee JK (2019) Neutrophil extracellular trap induced by HMGB1 exacerbates damages in the ischemic brain. Acta Neuropathol Commun. 7(1):94.

Kiran S (2012) What Is the Nature of Poststroke Language Recovery and Reorganization? ISRN Neurol. 2012:1–13.

Kwok ZH, Wang C, Jin Y (2021) Extracellular vesicle transportation and uptake by recipient cells: A critical process to regulate human diseases. Processes. 9(2):1–16.

Lai TW, Zhang S, Wang YT (2014) Excitotoxicity and stroke: Identifying novel targets for neuroprotection. Prog Neurobiol.115:157-88.

Latchaw RE, Yonas H, Hunter GJ, Yuh WTC, Ueda T, Sorensen AG, Sunshine JL, Biller J, Wechsler L, Higashida R, Hademenos G (2003) Guidelines and recommendations for perfusion imaging in cerebral ischemia: A scientific statement for healthcare professionals by the writing group on perfusion imaging, from the Council on Cardiovascular Radiology of the American Heart Association. Stroke. 34(4):1084–1104.

Lee MC, Kim RG, Lee T, Kim JH, Lee KH, Choi YD, Kim HS, Cho J, Park JY, Kim HI (2020) Ultrastructural Dendritic Changes Underlying Diaschisis After Capsular Infarct. J Neuropathol Exp Neurol. 79(5):508–517.

Léveillé F, Papadia S, Fricker M, Bell KFS, Soriano FX, Martel MA, Puddifoot C, Habel M, Wyllie DJ, Ikonomidou C, Tolkovsky AM, Hardingham GE (2010) Suppression of the intrinsic apoptosis pathway by synaptic activity. J Neurosci. 30(7):2623–2635.

Li L, Lundkvist A, Andersson D, Wilhelmsson U, Nagai N, Pardo AC, Nodin C, Ståhlberg A, Aprico K, Larsson K, Yabe T, Moons L, Fotheringham A, Davies I, Carmeliet P, Schwartz JP, Pekna M, Kubista M, Blomstrand F, … Pekny M (2008) Protective role of reactive astrocytes in brain ischemia. J Cereb Blood Flow Metab. 28(3):468–481.

Li P, Stetler RA, Leak RK, Shi Y, Li Y, Yu W, Bennett MVL, Chen J (2018) Oxidative stress and DNA damage after cerebral ischemia: Potential therapeutic targets to preserve the genome and improve stroke recovery. Neuropharmacology. 134(Pt B):208-217.

Li S, Overman JJ, Katsman D, Kozlov S V., Donnelly CJ, Twiss JL, Giger RJ, Coppola G, Geschwind DH, Carmichael ST (2010) An age-related sprouting transcriptome provides molecular control of axonal sprouting after stroke. Nat Neurosci. 13(12):1496-504.

Li T, Zhao J, Xie W, Yuan W, Guo J, Pang S, Gan WB, Gómez-Nicola D, Zhang S (2021) Specific depletion of resident microglia in the early stage of stroke reduces cerebral ischemic damage. J Neuroinflammation. 18(1):1–15.

Li Y, Zhang J-J, Chen R-J, Chen L, Chen S, Yang X-F, Min J-W (2022) Genistein mitigates oxidative stress and inflammation by regulating Nrf2/HO-1 and NF-κB signaling pathways in hypoxic-ischemic brain damage in neonatal mice. Ann Transl Med. 10(2):32–32.

Liauw J, Hoang S, Choi M, Eroglu C, Choi M, Sun GH, Percy M, Wildman-Tobriner B, Bliss T, Guzman RG, Barres BA, Steinberg GK (2008) Thrombospondins 1 and 2 are necessary for synaptic plasticity and functional recovery after stroke. J Cereb Blood Flow Metab. 28(10):1722–1732.

Liddelow SA, Barres BA (2017) Reactive Astrocytes: Production, Function, and Therapeutic Potential. Immunity. 46(6):957-967.

Liesz A, Zhou W, Mracskó É, Karcher S, Bauer H, Schwarting S, Sun L, Bruder D, Stegemann S, Cerwenka A, Sommer C, Dalpke AH, Veltkamp R (2011) Inhibition of lymphocyte trafficking shields the brain against deleterious neuroinflammation after stroke. Brain. 134(3):704–720.

Lin MP, Liebeskind DS (2016) Imaging of Ischemic Stroke. Contin Lifelong Learn Neurol. 22(5):1399–1423.

Ling C -M, Abdel-Latif AA (1968) Studies on Sodium Transport in Rat Brain Nerve-Ending Particles. J Neurochem. 15(8):721–729.

Liu R, Yuan H, Yuan F, Yang SH (2012) Neuroprotection targeting ischemic penumbra and beyond for the treatment of ischemic stroke. Neurol Res. 34(4):331–337.

Liu S, Levine SR, Winn R (2010) Targeting ischemic penumbra: part I - from pathophysiology to therapeutic strategy. J Exp Stroke Transl Med. 3(1):47-55.

Liu Y, Tak PW, Aarts M, Rooyakkers A, Liu L, Ted WL, Dong CW, Lu J, Tymianski M, Craig AM, Yu TW (2007) NMDA receptor subunits have differential roles in mediating excitotoxic neuronal death both in vitro and in vivo. J Neurosci. 27(11):2846–2857.

Liu Y, Xue X, Zhang H, Che X, Luo J, Wang P, Xu J, Xing Z, Yuan L, Liu Y, Fu X, Su D, Sun S, Zhang H, Wu C, Yang J (2019) Neuronal-targeted TFEB rescues dysfunction of the autophagy-lysosomal pathway and alleviates ischemic injury in permanent cerebral ischemia. Autophagy. 15(3):493–509.

Llovera G, Hofmann K, Roth S, Salas-Pérdomo A, Ferrer-Ferrer M, Perego C, Zanier ER, Mamrak U, Rex A, Party H, Agin V, Fauchon C, Orset C, Haelewyn B, De

Simoni MG, Dirnagl U, Grittner U, Planas AM, Plesnila N, … Liesz A (2015) Results of a preclinical randomized controlled multicenter trial (pRCT): Anti-CD49d treatment for acute brain ischemia. Sci Transl Med. 7(299):299ra121.

Lo Cicero A, Stahl PD, Raposo G (2015) Extracellular vesicles shuffling intercellular messages: for good or for bad. Curr Opin Cell Biol. 35:69–77.

Lo EH, Ning MM (2016) Mechanisms and challenges in translational stroke research. J Investig Med. 64(4):827–829.

Lodge KM, Cowburn AS, Li W, Condliffe AM (2020) The impact of hypoxia on neutrophil degranulation and consequences for the host. Int J Mol Sci. 21(4):1183.

Lossi L, Merighi A (2014) Neuronal cell death: Methods and protocols. Neuronal Cell Death Methods Protoc. 1254:1–368.

Love S (1999) Oxidative stress in brain ischemia. Brain Pathol. 9(1):119–131.

Manley GT, Zador Z, Stiver S, Wang V (2009) Role of aquaporin-4 in cerebral edema and stroke. Handb Exp Pharmacol. 190(190):159–170.

Martone ME, Jones YZ, Young SJ, Ellisman MH, Zivin JA, Hu BR (1999) Modification of Postsynaptic Densities after Transient Cerebral Ischemia: A Quantitative and Three-Dimensional Ultrastructural Study. J Neurosci. 19(6):1988–1997.

Matsuura T, Bureš J (1971) The minimum volume of depolarized neural tissue required for triggering cortical spreading depression in rat. Exp Brain Res 1971 123. 12(3):238–249.

McMeekin P, White P, James MA, Price CI, Flynn D, Ford GA (2017) Estimating the number of UK stroke patients eligible for endovascular thrombectomy. Eur Stroke J. 2(4):319–326.

Minamide LS, Striegl AM, Boyle JA, Meberg PJ, Bamburg JR (2000) Neurodegenerative stimuli induce persistent ADF/cofilin-actin rods that disrupt distal neurite function. Nat Cell Biol. 2(9):628–636.

Mulcahy LA, Pink RC, Carter DRF (2014) Routes and mechanisms of extracellular vesicle uptake. J Extracell Vesicles. 3(1).

Mussap M, Plebani M (2004) Biochemistry and clinical role of human cystatin C. Crit Rev Clin Lab Sci. 41(5–6):467–550.

Nakamura N, Rabouille C, Watson R, Nilsson T, Hui N, Slusarewicz P, Kreis TE, Warren G (1995) Characterization of a cis-Golgi matrix protein, GM130. J Cell Biol. 131(6 Pt 2):1715–1726.

Nakano T, Nishigami C, Irie K, Shigemori Y, Sano K, Yamashita Y, Myose T, Tominaga K, Matsuo K, Nakamura Y, Ishikura H, Kamimura H, Egawa T, Mishima K (2018) Goreisan Prevents Brain Edema after Cerebral Ischemic Stroke by Inhibiting Aquaporin 4 Upregulation in Mice. J Stroke Cerebrovasc Dis. 27(3):758–763.

Newman DJ (2002) Cystatin C. Ann Clin Biochem. 39(2):89–104.

Nian K, Harding IC, Herman IM, Ebong EE (2020) Blood-Brain Barrier Damage in Ischemic Stroke and Its Regulation by Endothelial Mechanotransduction. Front Physiol. 11:1681.

Nikonenko AG, Skibo GG (2004) Technique to quantify local clustering of synaptic vesicles using single section data. Microsc Res Tech. 65(6):287–291.

Orellana-Urzúa S, Rojas I, Líbano L, Rodrigo R (2020) Pathophysiology of Ischemic Stroke: Role of Oxidative Stress. Curr Pharm Des. 26(34):4246–4260.

Paciaroni M, Caso V, Agnelli G (2009) The concept of ischemic penumbra in acute stroke and therapeutic opportunities. Eur Neurol. 61(6):321–330.

Papayannopoulos V (2017) Neutrophil extracellular traps in immunity and disease. Nat Rev Immunol 2017 182. 18(2):134–147.

Perez-de-Puig I, Miró-Mur F, Ferrer-Ferrer M, Gelpi E, Pedragosa J, Justicia C, Urra X, Chamorro A, Planas AM (2015) Neutrophil recruitment to the brain in mouse and human ischemic stroke. Acta Neuropathol. 129(2):239–257.

Pérez-González R, Sahoo S, Gauthier SA, Kim Y, Li M, Kumar A, Pawlik M, Benussi L, Ghidoni R, Levy E (2019) Neuroprotection mediated by cystatin C-loaded extracellular vesicles. Sci Reports 2019 91. 9(1):1–10.

Phipps MS, Cronin CA (2020) Management of acute ischemic stroke. BMJ. 368:l6983.

Picone P, Porcelli G, Bavisotto CC, Nuzzo D, Galizzi G, Biagio PLS, Bulone D, Di Carlo M (2021) Synaptosomes: new vesicles for neuronal mitochondrial transplantation. J Nanobiotechnology. 19(1):6.

Prabhakaran S, Ruff I, Bernstein RA (2015) Acute stroke intervention: A systematic review. JAMA. 313(14):1451-62.

Puyal J, Clarke PGH (2009) Targeting autophagy to prevent neonatal stroke damage. Autophagy. 5(7):1060–1061.

Qin C, Zhou LQ, Ma XT, Hu ZW, Yang S, Chen M, Bosco DB, Wu LJ, Tian DS (2019) Dual Functions of Microglia in Ischemic Stroke. Neurosci Bull. 35(5):921-933.

Rabinstein AA (2020) Update on Treatment of Acute Ischemic Stroke. Contin Lifelong Learn Neurol. 26(2):268–286.

Rayasam A, Kijak JA, Kissel L, Choi YH, Kim T, Hsu M, Joshi D, Laaker CJ, Cismaru P, Lindstedt A, Kovacs K, Vemuganti R, Chiu SY, Priyathilaka TT, Sandor M, Fabry Z (2022) CXCL13 expressed on inflamed cerebral blood vessels recruit IL-21 producing TFH cells to damage neurons following stroke. J Neuroinflammation. 19(1):125.

Rodrigo R, Fernandez-Gajardo R, Gutierrez R, Matamala J, Carrasco R, Miranda-Merchak A, Feuerhake W (2013) Oxidative Stress and Pathophysiology of Ischemic Stroke: Novel Therapeutic Opportunities. CNS Neurol Disord - Drug Targets. 12(5):698–714.

Saint-Pol J, Gosselet F, Duban-Deweer S, Pottiez G, Karamanos Y (2020) Targeting and Crossing the Blood-Brain Barrier with Extracellular Vesicles. Cells. 9(4):851.

Sampedro MN, Bussineau CM, Cotman CW (1981) Postsynaptic density antigens: preparation and characterization of an antiserum against postsynaptic densities. J Cell Biol. 90(3):675-686.

Sattler R, Xiong Z, Lu WY, Hafner M, MacDonald JF, Tymianski M (1999) Specific coupling of NMDA receptor activation to nitric oxide neurotoxicity by PSD-95 protein. Science (80-). 284(5421):1845–1848.

Saver JL (2006) Time is brain - Quantified. Stroke. 37(1):263–266.

Sercombe L, Veerati T, Moheimani F, Wu SY, Sood AK, Hua S (2015) Advances and

challenges of liposome assisted drug delivery. Front Pharmacol. 6(DEC):286.
Sheikh AM, Wada Y, Tabassum S, Inagaki S, Mitaki S, Yano S, Nagai A (2021) Aggregation of cystatin c changes its inhibitory functions on protease activities and amyloid β fibril formation. Int J Mol Sci. 22(18):9682.
Shichita T, Sugiyama Y, Ooboshi H, Sugimori H, Nakagawa R, Takada I, Iwaki T, Okada Y, Iida M, Cua DJ, Iwakura Y, Yoshimura A (2009) Pivotal role of cerebral interleukin-17–producing γδT cells in the delayed phase of ischemic brain injury. Nat Med 2009 158. 15(8):946–950.
Shu L, Chen B, Chen B, Xu H, Wang G, Huang Y, Zhao Y, Gong H, Jiang M, Chen L, Liu X, Wang Y (2019) Brain ischemic insult induces cofilin rod formation leading to synaptic dysfunction in neurons. J Cereb Blood Flow Metab. 39(11):2181–2195.
Silva GS, Nogueira RG (2020) Endovascular Treatment of Acute Ischemic Stroke. Contin Lifelong Learn Neurol. 26(2):310–331.
Soltani MH, Pichardo R, Song Z, Sangha N, Camacho F, Satyamoorthy K, Sangueza OP, Setaluri V (2005) Microtubule-associated protein 2, a marker of neuronal differentiation, induces mitotic defects, inhibits growth of melanoma cells, and predicts metastatic potential of cutaneous melanoma. Am J Pathol. 166(6):1841–1850.
Stroemer RP, Kent TA, Hulsebosch CE (1995) Neocortical Neural Sprouting, Synaptogenesis, and Behavioral Recovery After Neocortical Infarction in Rats. Stroke. 26(11):2135–2144.
Sun MK, Xu H, Alkon DL (2002) Pharmacological protection of synaptic function, spatial learning, and memory from transient hypoxia in rats. J Pharmacol Exp Ther. 300(2):408–416.
Terasaki Y, Sasaki T, Yagita Y, Okazaki S, Sugiyama Y, Oyama N, Omura-Matsuoka E, Sakoda S, Kitagawa K (2010) Activation of NR2A receptors induces ischemic tolerance through CREB signaling. J Cereb Blood Flow Metab. 30(8):1441–1449.
Tizon B, Sahoo S, Yu H, Gauthier S, Kumar AR, Mohan P, Figliola M, Pawlik M, Grubb A, Uchiyama Y, Bandyopadhyay U, Cuervo AM, Nixon RA, Levy E (2010) Induction of Autophagy by Cystatin C: A Mechanism That Protects Murine Primary Cortical Neurons and Neuronal Cell Lines. PLoS One. 5(3):e9819.
Trivedi PC, Bartlett JJ, Pulinilkunnil T (2020) Lysosomal Biology and Function: Modern View of Cellular Debris Bin. Cells. 9(5):1131.
Ünal-Çevik I, Kilinç M, Gürsoy-Özdemir Y, Gurer G, Dalkara T (2004) Loss of NeuN immunoreactivity after cerebral ischemia does not indicate neuronal cell loss: A cautionary note. Brain Res. 1015(1–2):169–174.
van Niel G, Carter DRF, Clayton A, Lambert DW, Raposo G, Vader P (2022) Challenges and directions in studying cell–cell communication by extracellular vesicles. Nat Rev Mol Cell Biol. 23(5):369-382.
Van Niel G, D'Angelo G, Raposo G (2018) Shedding light on the cell biology of extracellular vesicles. Nat Rev Mol Cell Biol. 19(4):213–228.
Vrselja Z, Daniele SG, Silbereis J, Talpo F, Morozov YM, Sousa AMM, Tanaka BS, Skarica M, Pletikos M, Kaur N, Zhuang ZW, Liu Z, Alkawadri R, Sinusas AJ,

Latham SR, Waxman SG, Sestan N (2019) Restoration of brain circulation and cellular functions hours postmortem. Nature. 568(7752):336-343.

Vyklicky V, Korinek M, Smejkalova T, Balik A, Krausova B, Kaniakova M, Lichnerova K, Cerny J, Krusek J, Dittert I, Horak M, Vyklicky L (2014) Structure, function, and pharmacology of NMDA receptor channels. Physiol Res. 63(SUPPL.):191–203.

Walch-Solimena C, Blasi J, Edelmann L, Chapman ER, Von Mollard GF, Jahn R (1995) The t-SNAREs syntaxin 1 and SNAP-25 are present on organelles that participate in synaptic vesicle recycling. J Cell Biol. 128(4):637-645.

Wen M, Jin Y, Zhang H, Sun X, Kuai Y, Tan W (2019) Proteomic Analysis of Rat Cerebral Cortex in the Subacute to Long-Term Phases of Focal Cerebral Ischemia-Reperfusion Injury. J Proteome Res. 18(8):3099–3118.

Woitzik J, Hecht N, Pinczolits A, Sandow N, Major S, Winkler MKL, Weber-Carstens S, Dohmen C, Graf R, Strong AJ, Dreier JP, Vajkoczy P (2013) Propagation of cortical spreading depolarization in the human cortex after malignant stroke. Neurology. 80(12):1095–1102.

Wu QJ, Tymianski M (2018) Targeting nmda receptors in stroke: New hope in neuroprotection Tim Bliss. Mol Brain. 11(1):15.

Xie Q, Cheng J, Pan G, Wu S, Hu Q, Jiang H, Wang Y, Xiong J, Pang Q, Chen X (2019) Treadmill exercise ameliorates focal cerebral ischemia/reperfusion-induced neurological deficit by promoting dendritic modification and synaptic plasticity via upregulating caveolin-1/VEGF signaling pathways. Exp Neurol. 313:60–78.

Xiong XY, Liu L, Yang QW (2016) Functions and mechanisms of microglia/macrophages in neuroinflammation and neurogenesis after stroke. Prog Neurobiol. 142:23-44.

Xu B, Xiao AJ, Chen W, Turlova E, Liu R, Barszczyk A, Sun CLF, Liu L, Tymianski M, Feng ZP, Sun HS (2016) Neuroprotective Effects of a PSD-95 Inhibitor in Neonatal Hypoxic-Ischemic Brain Injury. Mol Neurobiol. 53(9):5962–5970.

Yan W, Fan J, Zhang X, Song H, Wan R, Wang W, Yin Y (2021) Decreased neuronal synaptosome associated protein 29 contributes to poststroke cognitive impairment by disrupting presynaptic maintenance. Theranostics. 11(10):4616–4636.

Yáñez-Mó M, Siljander PRM, Andreu Z, Zavec AB, Borràs FE, Buzas EI, Buzas K, Casal E, Cappello F, Carvalho J, Colás E, Cordeiro-Da Silva A, Fais S, Falcon-Perez JM, Ghobrial IM, Giebel B, Gimona M, Graner M, Gursel I, … De Wever O (2015) Biological properties of extracellular vesicles and their physiological functions. J Extracell Vesicles. 4(2015):1–60.

Yang B, Xu J, Chang L, Miao Z, Heang D, Pu Y, Zhou X, Zhang L, Xie H (2020) Cystatin C improves blood-brain barrier integrity after ischemic brain injury in mice. J Neurochem. 153(3):413–425.

Yang C, Wang X (2021) Lysosome biogenesis: Regulation and functions. J Cell Biol. 220(6):e202102001.

Yang SH, Liu R (2021) Four Decades of Ischemic Penumbra and Its Implication for Ischemic Stroke. Transl Stroke Res. 12(6):937–945.

Zhang Q, Gao T, Luo Y, Chen X, Gao G, Gao X, Zhou Y, Dai J (2012) Transient Focal Cerebral Ischemia/Reperfusion Induces Early and Chronic Axonal Changes in Rats: Its Importance for the Risk of Alzheimer's Disease. PLoS One. 7(3):e33722.

Zhang X, Wei M, Fan J, Yan W, Zha X, Song H, Wan R, Yin Y, Wang W (2021) Ischemia-induced upregulation of autophagy preludes dysfunctional lysosomal storage and associated synaptic impairments in neurons. Autophagy. 17(6):1519-1542.

Zhang X, Zhang Q, Tu J, Zhu Y, Yang F, Liu B, Brann D, Wang R (2015) Prosurvival NMDA 2A receptor signaling mediates postconditioning neuroprotection in the hippocampus. Hippocampus. 25(3):286–296.

Zhang Y, Wu Z, Huang Z, Liu Y, Chen X, Zhao X, He H, Deng Y (2022) GSK-3β inhibition elicits a neuroprotection by restoring lysosomal dysfunction in neurons via facilitation of TFEB nuclear translocation after ischemic stroke. Brain Res. 1778:147768.

Zhang Z, Cao X, Bao X, Zhang Y, Xu Y, Sha D (2020) Cocaine- and amphetamine-regulated transcript protects synaptic structures in neurons after ischemic cerebral injury. Neuropeptides. 81:102023.

Zhu L, Wang L, Ju F, Ran Y, Wang C, Zhang S (2017) Transient global cerebral ischemia induces rapid and sustained reorganization of synaptic structures. J Cereb Blood Flow Metab. 37(8):2756-2767.

Acknowledgment

Thanks to my scientific mother, PD Dr. rer nat. Berta Puig. I always feel glad that I have you as my supervisor at this stage of my life. Before starting my doctoral study, my knowledge of basic scientific work was very poor. Your guidance has covered not only the details of lab work but also the essence of scientific spirit, which is the combination of organization, prudence and patience. When I have doubts in work, you always offer me good advice or point out new directions. Besides, you are also a good friend, caring about the obstacles and upsets that I came across from time to time in my life and ready to support me whenever I need.

Thanks to my scientific father, Prof. Dr. med. Tim Magnus. You are an accommodating leader, providing us a nice working environment and the opportunities to improve ourselves. During my doctoral study, you offered me important support and advice like how to be a good presenter.

Many thanks to my colleagues, Haodi Cai, Hind Haj Ahmad, Lennart Pöls, Mingming Zha, Javier Randez Garbayo, Jasmin Pabla, Katrin Lessmann, Karoline Degenhardt, Santra Brenna, and Sara Isla Cainyos, I feel privileged to work with you guys, as you are all kind, helpful and studious people. From you, I get the chance to see different lifestyles and learn to touch different aspects of life.

Thanks to all my collaborators, Professor Efrat Levy, Yohan Kim, Dr. Virgilio Failla, Hannah Voß, Christoph Krisp, Michaela Schweizer, Chudamani Raithore, and Julia Biermann. The technical and experimental support I got from you helped me to go on with my research and improved my understanding of other dimensions of scientific work.

I also want to express my gratitude toward my motherland, China. It was the sponsor from the Chinese Scholarship Council initially offered me the chance to further my medical doctoral study in such a good academic institution: Universitätesklinikum Hamburg-Eppendorf, Hamburg, Germany.

Furthermore, I need to thank the Werner Otto Scholarship committee, they gave me the chance to extend the duration of my doctoral study, without their support, I cannot make the progress on the research I have made so far and my doctoral study would have been not complete.

Last but not least, I want to thank the Asia shops and restaurants in Hamburg, the local Chinese food ingredients and dishes they sell is a kind of important consolation for me during the last three years. I knew I am a person who enjoys eating, after this three years, I realize that eating food from my homeland is an indispensable part of my life.

Resume

Lebenslauf entfällt aus datenschutzrechtlichen Gründen.

Declaration on oath

Hiermit versichere ich, dass diese Dissertation von mir ohne fremde Hilfe verfasst wurde, mit Ausnahme der angegebenen. Und ich versichere Ihnen, dass diese Dissertation weder einem Facharzt an einer anderen Universität zur Begutachtung noch zur Bewerbung um die Zulassung zur Promotion vorgelegt wurde.

Ich erkläre mich einverstanden, dass meine Dissertation vom Dekanat der Medizinischen Fakultät mit einer gängigen Software zur Erkennung von Plagiaten überprüft werden kann.

Date: Signature: